

**TEAR FILM DYNAMICS IN BREAKUP
WITH A ROUGH OCULAR SURFACE**

by

Amy E. Janett

A thesis submitted to the Faculty of the University of Delaware in partial fulfillment of the requirements for the degree of Master of Science in Applied Mathematics

Summer 2016

© 2016 Amy E. Janett
All Rights Reserved

ProQuest Number: 10190958

All rights reserved

INFORMATION TO ALL USERS

The quality of this reproduction is dependent upon the quality of the copy submitted.

In the unlikely event that the author did not send a complete manuscript and there are missing pages, these will be noted. Also, if material had to be removed, a note will indicate the deletion.



ProQuest 10190958

Published by ProQuest LLC (2016). Copyright of the Dissertation is held by the Author.

All rights reserved.

This work is protected against unauthorized copying under Title 17, United States Code
Microform Edition © ProQuest LLC.

ProQuest LLC.
789 East Eisenhower Parkway
P.O. Box 1346
Ann Arbor, MI 48106 - 1346

**TEAR FILM DYNAMICS IN BREAKUP
WITH A ROUGH OCULAR SURFACE**

by

Amy E. Janett

Approved: _____
Richard J. Braun, Ph.D.
Professor in charge of thesis on behalf of the Advisory Committee

Approved: _____
Louis Rossi, Ph.D.
Chair of the Department of Mathematical Sciences

Approved: _____
George H. Watson, Ph.D.
Dean of the College of Arts and Sciences

Approved: _____
Ann L. Ardis, Ph.D.
Senior Vice Provost for Graduate and Professional Education

ACKNOWLEDGMENTS

I am deeply grateful for the immense support and encouragement I've received from my thesis advisor, Dr. Richard Braun. Thank you for always believing in me. I cherish all that I've learned from working with you.

Thank you to my other committee members, Drs. Tobin Driscoll and Pak-Wing Fok, for constructive edits and for teaching me much of the background of this thesis in classes I've taken from you. A special thanks to Drs. Nayantara Bhatnagar and Michelle Cirillo for being strong advocates for me, for women in mathematics, and for AWM. To everyone who makes this department a better place – Deborah See, David Caldwell, Dr. Cristina Bacuta, and too many graduate students to list – thank you for brightening many of my days.

I'm fortunate to have such loving and supportive family members, who always keep me optimistic during my biggest struggles. Thank you Mom, Dad, Mark, and Grandma for always being proud, even if you don't understand what I'm doing.

I owe endless gratitude to Madelyn Houser, my brilliant classmate, best friend, and biggest supporter throughout graduate school. Without you, none of this would be possible. Thank you for celebrating with me in good times, helping me through bad times, and always providing the perfect balance of goofing off and rigorously discussing mathematics together. On top of everything we learned in class, we started an AWM chapter from scratch and it grew into something bigger and better than we ever hoped. I love you.

TABLE OF CONTENTS

LIST OF TABLES	vi
LIST OF FIGURES	vii
ABSTRACT	x
 Chapter	
1 INTRODUCTION	1
2 PROBLEM FORMULATION	8
2.1 Modeling Assumptions	8
2.2 Governing Equations Overview	10
2.2.1 Equations for Interior	10
2.2.2 Boundary Conditions at Corneal Surface	10
2.2.3 Boundary Conditions at Free Surface	10
2.3 Equations for Interior	11
2.4 Equation for Corneal Surface	14
2.5 Boundary Conditions	15
2.5.1 Corneal Surface	15
2.5.2 Free Surface	16
2.6 Governing Equations in Thin Film Limit	20
2.7 Reduction	21
3 NUMERICAL DISCRETIZATION	25
4 RESULTS	28
4.1 Effect of Corneal Surface Features	28
4.2 Effect of Wetting Forces	42

5 DISCUSSION AND CONCLUSIONS	50
BIBLIOGRAPHY	53
Appendix	
A PERMISSION LETTERS	56
A.1 Permission from Wolters Kluwer Health	56
A.2 Permission from Elsevier	60

LIST OF TABLES

2.1	Dimensional Parameters	12
2.2	Dimensionless Parameters	12
4.1	Ratio of tear film amplitude to corneal surface amplitude ($r = h_{amp}/z_a$) for various ocular surface functions. The amplitude of the tear film corresponding to the two wave corneal surface is larger than the $k = 20$ amplitude and smaller than the $k = 5$ amplitude. This further suggests that the inclusion of shorter waves has a flattening effect.	41
4.2	Wavenumber for various ocular surface functions. We note that these values are approximate due to the numerical discretization process and the fact that the tear film surface is not truly periodic. We observe a longer wave for the two-wave case, close to $k = 5$, and we do not see the $k = 20$ wave.	42
4.3	Comparison of van der Waals' disjoining pressure, and Dai et al.'s disjoining pressure for films of nonuniform thickness.	49

LIST OF FIGURES

1.1	Diagram of the tear film. The region labeled “Mucin Layer” is what we refer to as the glycocalyx.	1
1.2	Panel of images of the tear film before and after blinks. In panel A, before downstroke the authors use arrows to highlight abnormalities, which are likely bubbles, in the lipid layer. Panel B is taken during the downstroke and four dots appear in the rectangle. In panel C, another downstroke about one minute later, we observe the four dots again in the same position as in panel C, suggesting they are an artifact of the corneal surface. Panel D is taken during upstroke and the four dots are in the same position but with flow on the opposite side from panels B & C. From figure 4 of [1].	4
1.3	Rough texture visible in interferometric imaging of the lipid layer. We focus on the type of roughness visible in the streaks (arrowhead). Other types of roughness visible in this image are small spots (arrows) and larger patches (asterisk). From figure 3 of [2].	5
1.4	Rough texture visible in retroillumination imaging of the lipid layer. The roughness becomes stronger as the interblink time increases. From figure 26 of [1].	6
2.1	A schematic of the problem set-up, with dimensional variables indicated by primes. The thickness of the aqueous layer is h' , the corneal surface is modeled by z'_c , and evaporation is given by J' . . .	9
4.1	Time series plots of aqueous layer thickness with sinusoidal corneal surface (left) vs. flat corneal surface (right). The model exhibits the same behavior up until time $t = t_{\text{end}}$ (dimensionless 1.07; dimensional 11.24s), at which time the film anterior to the rough surface develops ripples at TBU. The film anterior to the flat corneal surface also reaches TBU, but with no ripples.	29

4.2	Comparison of tear film dynamics with varying corneal surface wavenumber. The first three subplots contain numerical results for $k = 5$, $k = 10$, and $k = 20$, respectively, with the corneal surface plotted at the bottom of each figure in blue. Solution curves represent the location of the free surface at each time step. Time starts at $t = 0$, increasing by 0.1 until final time $t = 0.8821$. As t increases, $h + z_c$ decreases monotonically. The final figure compares the tear film at TBU with each wavenumber.	31
4.3	Procedure for finding the approximate tear film amplitude.	32
4.4	Ratio of the tear film amplitude to the corneal surface amplitude as a function of corneal surface wavenumber. Tear film roughness decreases as the wavenumber increases. At the default wavenumber $k = 10$, the ratio is less than 0.06. At $k = 5$, the TBU tear film amplitude to corneal surface amplitude is its highest at almost 0.2.	33
4.5	Quadratic polynomial fit, given by (4.1) (red curve) plotted with simulation data for the wavelengths corresponding to integer wavenumbers (blue circles).	34
4.6	Nonlinear curve fit of the ratio values plotted as the red line, with the ratio values plotted as blue circles.	36
4.7	Amplitude of the tear film versus the amplitude of the corneal surface when $k = 10$. We obtain the largest amplitude for the default ocular surface amplitude $z_a = 1/14$, contrasting with the relative amplitude case in which the largest r value occurred at $z_a = 0.025$	37
4.8	Nonlinear curve fit of the ratio values plotted as the red line, with the ratio values plotted as blue circles.	38
4.9	Amplitude of the tear film versus the amplitude of the corneal surface when $k = 5$. We obtain the largest amplitude for the ocular surface amplitude $z_a = 0.15$	39
4.10	Final four time steps (from $t = 0.6$, increasing by 0.1 until final time of $t = 0.8791$) of the tear film in a localized region where TBU occurs, with decreasing thickness throughout time. The tear film ripples in the final time step at TBU, with the wavelength appearing to echo the longer waves ($k_1 = 5$) but not the shorter waves ($k_2 = 20$).	40

4.11	Left plot: time series plot of film thickness with absence of wetting forces. Top blue curve is $t = 0$; bottom teal curve is $t = .9291$. The tear film thins until the solver stops it at $h_{min} = 10^{-2}$. In this case, there are no visible ripples in the tear film. Right plot: the same model simulation, zoomed into the localized region at which TBU occurs.	44
4.12	Time series plot of film thickness with van der Waals' wetting forces. Top blue curve is $t = 0$; time increases by 0.1 until the bottom purple curve at $t = 1.0015$. The tear film thins until the solver stops it at thickness $h = 10^{-2}$. The wetting forces cause the tear film to spread across the corneal surface at TBU, echoing the shape of the surface.	45
4.13	Ratio of the tear film amplitude to the corneal surface amplitude as a function of wavenumber when TBU is defined as $\min_x h(x, t) = 10^{-2}$.	46
4.14	Time series plot of film thickness with wetting forces governed by (4.12). Starting with time $t = 0$, we increase by 0.1 until the final time of $t = 1.0134$. We obtain the same behavior with (4.12) as with (4.8).	48

ABSTRACT

Experimental images of the tear film have been found to contain areas of rough texture. For long interblink times, the rough areas become more pronounced. We model tear film dynamics during the interblink. As the film thins to a critically low thickness, tear breakup (TBU) occurs. We hypothesize that the rough areas in experimental imaging are artifacts of the corneal surface, visible during TBU. To explore our hypothesis, we use one-dimensional thin film equations to model tear film fluid flow, and model the corneal surface as a sinusoidal function to account for its roughness. We use Fourier spectral methods to discretize in space and solve the resulting differential algebraic system using backward differentiation methods in Matlab. We parametrically study the effect of corneal surface features and of wetting forces on the tear film dynamics at TBU. Our results suggest that tear film rippling occurs at, but not before, TBU, and they support the interpretation of rough texture in experimental imaging as evidence of corneal surface roughness appearing during TBU.

Chapter 1

INTRODUCTION

The tear film is a multilayered thin fluid that covers and protects the surface of the eye. The anterior layer is a lipid layer which slows evaporation of the aqueous layer [3]. The aqueous layer constitutes the majority of the tear film and lies posterior to the lipid layer. Posterior to the aqueous layer is the glycocalyx, a forest of transmembrane mucins protruding from the ocular surface into the aqueous layer [4]. The ocular surface, specifically of the cornea, comprises multiple layers of epithelial cells. These cells vary in width and height, forming a rough surface [5, 6, 7]. Figure 1.1, from [8], contains a diagram of the tear film.

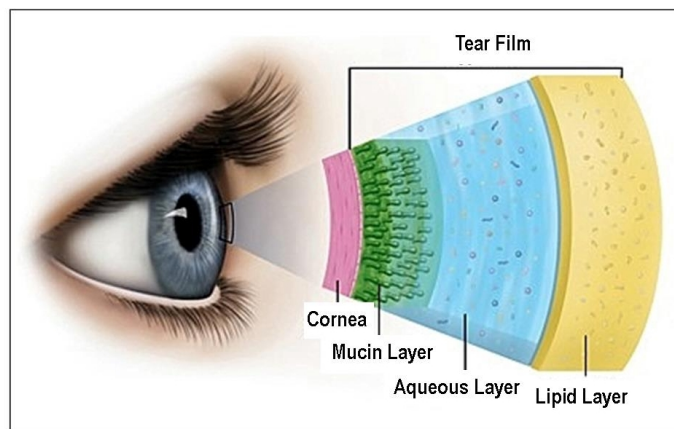


Figure 1.1: Diagram of the tear film. The region labeled “Mucin Layer” is what we refer to as the glycocalyx.

Maintaining a healthy tear film thickness is critical for proper vision. Early measurements of the aqueous layer estimated it to be 7 microns thick [9]. However, recent studies with more accurate measurements have estimated an average healthy aqueous layer to be between $1.5 - 4.7\mu\text{m}$ thick, with an average of $3\mu\text{m}$ [10]. When the tear film thins to a critically small thickness, tear break-up (TBU) occurs. [11]. TBU is a common phenomenon associated with dry eye, a condition that affects over three million Americans per year [12]. The causes of TBU are not very well-understood, and may be a result of a variety of mechanisms including increased evaporation and the Marangoni effect [13]. Initial studies investigating the effect of evaporation on tear film thinning determined that evaporation speed was not adequately fast to result in TBU [3]. However, such studies were based on the assumption that the aqueous layer is 7 microns thick, and were conducted using experimental goggles which may inadvertently slow evaporation. Given the newer and lower aqueous layer thickness estimate, along with proposed faster evaporation in outside air without experimental goggles, evaporation becomes a plausible candidate for the mechanism behind TBU [1, 2, 14, 15].

The role of evaporation in TBU is linked to the health and function of the lipid layer. During a blink, the upper eyelid drives fluid flow of the tear film and redistributes the lipid layer across the film [1]. In a healthy tear film, the lipid layer maintains a thickness of about 0.1 microns [9]. The lipid layer slows evaporation of the aqueous layer so that the tear film maintains a sufficient thickness between blinks [3]. When the lipid layer develops a thin region, which we call a hole, evaporation increases in the problematic region and drives local thinning of the film [16]. We explore herein the situation in which TBU occurs due to increased evaporation as a function of a hole in the lipid layer.

We are particularly interested in building on the work of Braun et al. in [1], in which tear film dynamics during the blink cycle are modeled using a rough corneal

surface. The blink cycle consists of four parts: the downstroke during which the superior lid moves towards the inferior lid, the turning point where the superior lid stops, the upstroke during which the superior lid moves away from the inferior lid, and the interblink period in between the previous upstroke and next downstroke. Braun et al.'s research suggests that the ocular surface roughness is visible in the tear film during a blink based on the fluid motion over the ocular surface. Experimental images and model results show matching of peak to valley in the tear film and ocular surface based on the direction the fluid is moving over the surface [1]. Their work was motivated by images of the tear film taken during and between blinks, such as figure 1.2. These images were taken using interferometry, a technique which uses the phase difference between different reflections of light off the tear film surfaces to measure lipid layer thickness. The thickness is then represented with a color spectrum scale. Figure 1.2 is a grayscale of the original interferometric image.

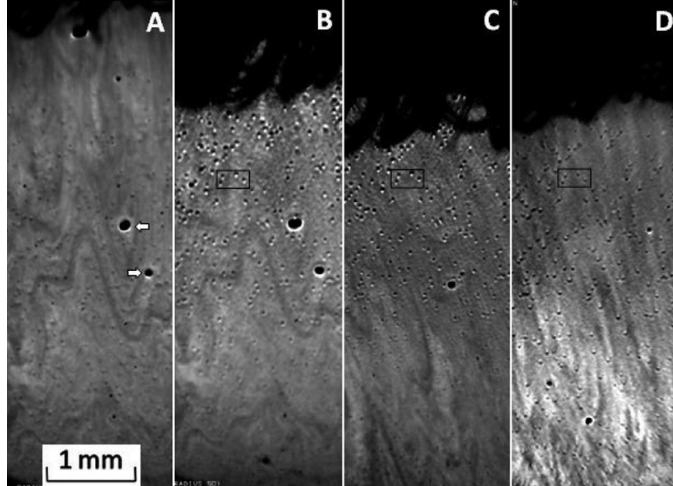


Figure 1.2: Panel of images of the tear film before and after blinks. In panel A, before downstroke the authors use arrows to highlight abnormalities, which are likely bubbles, in the lipid layer. Panel B is taken during the downstroke and four dots appear in the rectangle. In panel C, another downstroke about one minute later, we observe the four dots again in the same position as in panel C, suggesting they are an artifact of the corneal surface. Panel D is taken during upstroke and the four dots are in the same position but with flow on the opposite side from panels B & C. From figure 4 of [1].

While [1] modeled the effect of corneal surface roughness on tear film dynamics during a blink, we aim to understand the effect of corneal surface roughness on tear film dynamics during interblink, and more specifically at TBU. Images such as figure 1.3 motivate our work; such images capture a rough texture on localized regions of the tear film. In figure 1.3, King-Smith et al. [2] took monochrome, narrow band laser interferometric images of the tear film during the interblink phase. Ripples in the tear film are also visible in images such as figure 1.4, which measure changes in tear film slope by a light that enters the eye [1]. The changes in slope are then integrated to

obtain a thickness measurement. The rough texture observed in such images during interblink serves as a motivation for our model.

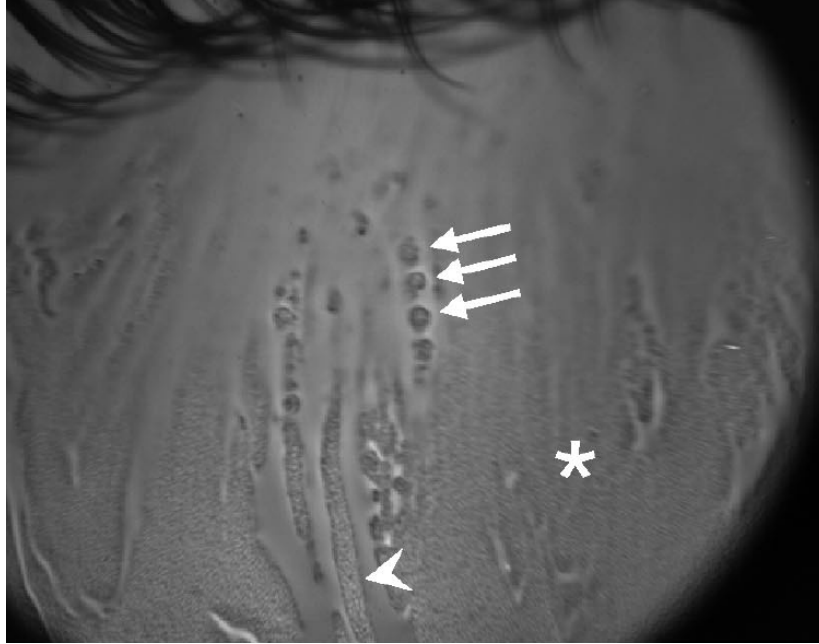


Figure 1.3: Rough texture visible in interferometric imaging of the lipid layer. We focus on the type of roughness visible in the streaks (arrowhead). Other types of roughness visible in this image are small spots (arrows) and larger patches (asterisk). From figure 3 of [2].

In order to effectively model the tear film, we introduce several simplifications to its physiology while capturing the key components of the system. We simplify the tear film to be a single aqueous layer and model it in one spatial dimension. As previously stated, a hole in the lipid layer corresponds to heightened evaporation at the location of the hole. Thus we account for the protective effect of a healthy lipid layer using an evaporation function with a small background evaporation rate and a localized increased evaporation rate. Many previous models assume the corneal surface to be flat [17], with the effect of curvature negligible because the thickness of the local segment of tear film is two orders of magnitude smaller than the tear film diameter [18]. This

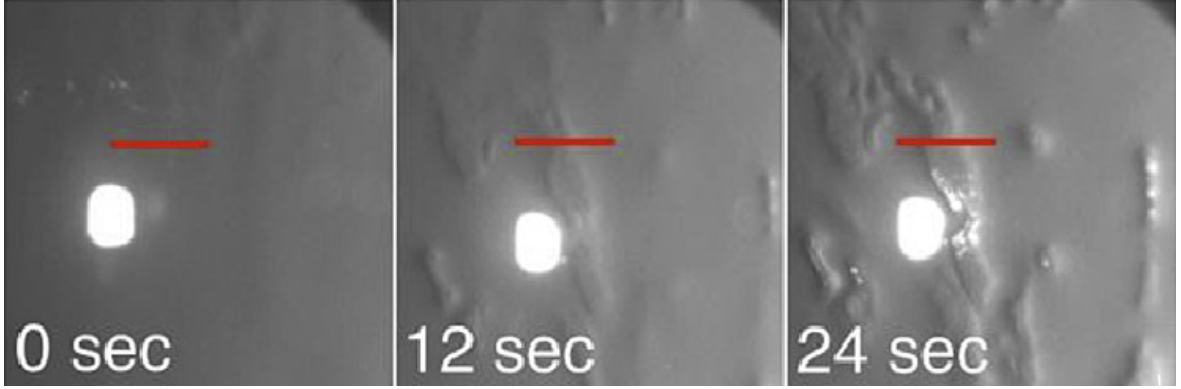


Figure 1.4: Rough texture visible in retroillumination imaging of the lipid layer. The roughness becomes stronger as the interblink time increases. From figure 26 of [1].

modeling simplification is justified when exploring the tear film in general, as the effect of the corneal surface roughness is trumped by the free surface curvature in the case of a healthy film thickness. But when the tear film thins in the case of TBU, conjonjunctival pressure pushes the fluid-solid interface away from the fluid-air interface, resulting in the spread of the film over the corneal surface. Moreover, as we will show in the results section, there is no substantial change in pre-TBU thinning rate between the case of a flat or rough corneal surface. However, given that we are investigating the roughness visible in TBU images, we choose to model the corneal surface as a sinusoidal function and parameters to account for the variation in epithelial cells and ocular surface roughness.

Our use of a sinusoidal function for surface roughness builds on previous work in flow over topography [19]. Kalliadas et al. [20] develop a model for thin film flow over a step, demonstrating how the film forms a capillary ridge immediately before the step drops down in height. The stability of such results and the justification of using a lubrication approximation for the thin film equations in the case of a rough topography has been explored as well [21]. The work of [20, 21] has been extended to the case of

a sinusoidal substrate in [22], which we also use.

We quantitatively investigate the presence or absence of roughness in the tear film before and during TBU. Parameters that we explore include corneal epithelial cell height, cell thickness, and wetting forces. We present the problem formulation in chapter 2, outlining the theoretical framework of our model. In chapter 3, we describe the process of numerical discretization and the numerical methods used to approximate model solutions. We present results in chapter 4, quantifying roughness of the tear film at TBU. Finally, we end with discussion and conclusions in chapter 5.

Chapter 2

PROBLEM FORMULATION

2.1 Modeling Assumptions

In order to obtain a simplified model, we must make some assumptions about the tear film. When functioning properly, the lipid layer retards evaporation of the aqueous layer. A common cause of tear film thinning is the presence of a relatively thin area of the lipid layer, which we call a hole [16]. Therefore, when modeling the tear film as a single aqueous layer, we account for the protective function of the lipid layer, along with holes in the lipid layer, by introducing a smooth evaporation function with peak evaporation in the center of the domain and a slower background evaporation rate elsewhere. Moreover, we assume that the aqueous layer of the tear film is Newtonian, in other words, that its viscous stresses are linearly proportional to the strain rate. We also assume that the aqueous layer is incompressible; that is, it has constant density ρ .

We begin by defining characteristic parameters relevant to our model, first with those that have been calculated or derived experimentally. Let $d = 3.5\mu\text{m}$ be the characteristic thickness in the spatial variable z' , based on the experimental average tear film thickness [10]. Furthermore, we assume that the tear-air interface has constant surface tension $\sigma_0 = 0.045\text{N/m}$, $\mu = 1.3 \times 10^{-3}\text{Pa}\cdot\text{s}$ is the constant viscosity of the tear film, and $v_0 = 20\mu\text{m}/\text{min}$ is the characteristic peak thinning rate [23, 24, 25]. We define a dimensionless parameter

$$S = \frac{\sigma_0 \varepsilon^4}{\mu v_0} \tag{2.1}$$

which provides a ratio of surface tension to viscosity, so that choosing $S = 1$ balances surface tension and viscous effects. Finally, we define $\varepsilon = d/L$ to be the ratio of characteristic height to length scale in the lateral direction. We solve for the characteristic length scale when $S = 1$ to obtain that

$$L = (\sigma_0/\mu v_0)^{1/4}d. \quad (2.2)$$

The resulting value for $L \approx 350\mu\text{m}$ in the spatial variable x' . We then choose the dimensional length scale to be $x_L L$, where $x_L = 8$, chosen large enough to capture a centered region of increased evaporation with slower evaporation on the sides.

We provide an illustration of the model set-up and domain in figure 2.1.

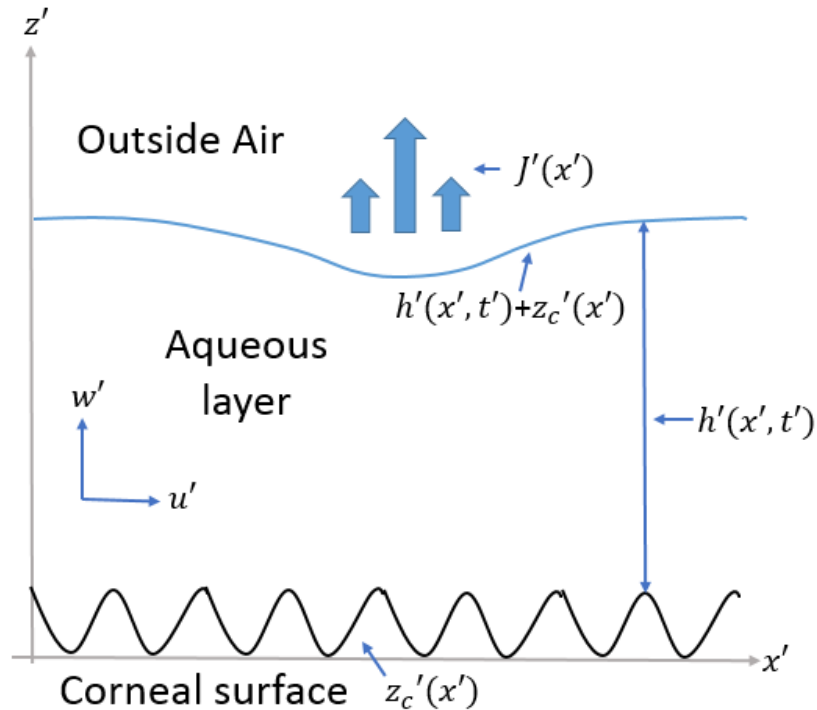


Figure 2.1: A schematic of the problem set-up, with dimensional variables indicated by primes. The thickness of the aqueous layer is h' , the corneal surface is modeled by z'_c , and evaporation is given by J' .

2.2 Governing Equations Overview

We present a list of the governing equations which we will use to derive our model PDEs. Primes denote dimensional variables. In the sections that follow, we describe these equations in greater detail and nondimensionalize them. Let $\mathbf{u}' = (u', w')$ denote velocity in the x' and z' direction, respectively, and p' be a scalar function representing pressure.

2.2.1 Equations for Interior

We conserve momentum and mass using the incompressible Navier-Stokes equations [26], namely

$$\rho \frac{\partial \mathbf{u}'}{\partial t'} + \mathbf{u}' \cdot \nabla \mathbf{u}' = -\nabla p' + \mu \nabla^2 \mathbf{u}', \quad (2.3)$$

$$\nabla \cdot \mathbf{u}' = 0. \quad (2.4)$$

2.2.2 Boundary Conditions at Corneal Surface

The no slip and impermeability conditions are

$$\mathbf{u}' \cdot \mathbf{t}'_c = 0, \quad (2.5)$$

$$\mathbf{u}' \cdot \mathbf{n}'_c = 0. \quad (2.6)$$

2.2.3 Boundary Conditions at Free Surface

Tangential immobility, the kinematic condition, and the normal stress condition are, respectively,

$$\mathbf{u}' \cdot \mathbf{t}' = 0, \quad (2.7)$$

$$\rho(\mathbf{u}' - \mathbf{u}'_I) \cdot \mathbf{n}' = J', \quad (2.8)$$

$$-p'_v - \mathbf{n}' \cdot \mathbf{T}' \cdot \mathbf{n}' = \sigma_0 \nabla' \cdot \mathbf{n}' - \Pi'(h'). \quad (2.9)$$

2.3 Equations for Interior

We assume that the tear film is incompressible, which we express with the equation

$$\nabla \cdot \mathbf{u}' = 0. \quad (2.10)$$

In Cartesian coordinates, (2.10) is written as

$$\frac{\partial u'}{\partial x'} + \frac{\partial w'}{\partial z'} = 0. \quad (2.11)$$

We note that (2.11) conserves mass. Moreover, the tear film is viscous so we can apply the Navier-Stokes equations to describe the fluid motion and conserve momentum:

$$\rho \frac{\partial \mathbf{u}'}{\partial t'} + \mathbf{u}' \cdot \nabla \mathbf{u}' = -\nabla p' + \mu \nabla^2 \mathbf{u}'. \quad (2.12)$$

In Cartesian coordinates, the components of (2.12) become

$$\rho \frac{\partial u'}{\partial t'} + u' \frac{\partial u'}{\partial x'} + w' \frac{\partial u'}{\partial z'} = -\frac{\partial p'}{\partial x'} + \mu \frac{\partial^2 u'}{\partial x'^2} + \mu \frac{\partial^2 u'}{\partial z'^2}, \quad (2.13)$$

$$\rho \frac{\partial w'}{\partial t'} + u' \frac{\partial w'}{\partial x'} + w' \frac{\partial w'}{\partial z'} = -\frac{\partial p'}{\partial z'} + \mu \frac{\partial^2 w'}{\partial x'^2} + \mu \frac{\partial^2 w'}{\partial z'^2}. \quad (2.14)$$

We nondimensionalize as follows:

$$u = u' \varepsilon / v_0, \quad w = w' / v_0, \quad p = (p' - p'_v) / p_0, \quad \text{where } p_0 = \frac{v_0 \mu}{\varepsilon^2 d}, \quad (2.15)$$

$$t = t' v_0 / d, \quad x = x' / L, \quad \text{and } z = z' / d.$$

In 2.15, p'_v is the reference environmental vapor pressure. Values for the dimensional parameters in (2.15) can be found in table 2.1. Additionally, we introduce a dimensionless parameter $\varepsilon := d/L$. This is the aspect ratio, which is small (see table 2.2).

We begin the process of nondimensionalization with (2.11):

$$\frac{v_0}{d} \frac{\partial u}{\partial x} + \frac{v_0}{d} \frac{\partial w}{\partial z} = 0. \quad (2.16)$$

Dividing by $\frac{v_0}{d}$, we obtain that

$$\frac{\partial u}{\partial x} + \frac{\partial w}{\partial z} = 0. \quad (2.17)$$

Table 2.1: Dimensional Parameters

Parameter	Definition	Value	Source
μ	Viscosity	$1.3 \times 10^{-3} \text{Pa}\cdot\text{s}$	[24]
ρ	Density	$10^3 \text{kg}\cdot\text{m}^{-3}$	Water
σ_0	Surface Tension	0.045N/m	[23]
v_0	Peak Thinning Rate	$20 \mu\text{m}/\text{min}$	[25]
v_1	Background Thinning Rate	$1 \mu\text{m}/\text{min}$	[25]
d	Characteristic Thickness	$3.5 \times 10^{-6} \text{m}$	[10]
L	$(\sigma_0/\mu/v_0)^{1/4}d$	$3.5 \times 10^{-4} \text{m}$	Calculated
A^*	Hamaker Constant	$6\pi \times 3.5 \times 10^{-19} \text{m}^3 \text{Pa}$	[27]
z'_a	Epithelial Cell Height	$0.25 \times 10^{-6} \text{m}$	[7]
λ'	Epithelial Cell Width	$35 \times 10^{-6} \text{m}$	[6]

Table 2.2: Dimensionless Parameters

Parameter	Definition	Value
ε	d/L	9.9×10^{-3}
Re	$\rho v_0 d / (\varepsilon^2 \mu)$	9.1×10^{-3}
k	L/λ'	10
A	$A^*/(6\pi\mu v_0 L^2)$	9.9×10^{-3}
S	$\sigma_0 \varepsilon^4 / (\mu v_0)$	1

Next, we write (2.13) in terms of dimensionless variables, noting that

$$\frac{\partial p'}{\partial x'} = \frac{\partial}{\partial x'} (p' - p'_v) \quad (2.18)$$

since p'_v is a constant. This allows us to substitute the dimensionless pressure into the following momentum equation:

$$\rho \left(\frac{v_0^2}{\varepsilon d} \frac{\partial u}{\partial t} + \frac{v_0^2}{d\varepsilon} \frac{\partial u}{\partial x} + \frac{v_0^2}{d\varepsilon} \frac{\partial u}{\partial z} \right) = -\frac{p_0}{L} \frac{\partial p}{\partial x} + \frac{\mu v_0}{\varepsilon L^2} \frac{\partial^2 u}{\partial x^2} + \frac{\mu v_0}{\varepsilon d^2} \frac{\partial^2 u}{\partial z^2}. \quad (2.19)$$

Multiplying by $\frac{d^2}{v_0 \varepsilon \mu}$, and using the fact that $\text{Re} = \frac{\rho v_0 d}{\varepsilon^2 \mu}$, we have

$$\text{Re} \left(\frac{\partial u}{\partial t} + u \frac{\partial u}{\partial x} + w \frac{\partial u}{\partial z} \right) = -\frac{1}{\varepsilon^2} \frac{\partial p}{\partial x} + \frac{\partial^2 u}{\partial x^2} + \frac{1}{\varepsilon^2} \frac{\partial^2 u}{\partial z^2}. \quad (2.20)$$

Multiplying by ε^2 , we obtain the following dimensionless PDE for u :

$$\varepsilon^2 \text{Re} \left(\frac{\partial u}{\partial t} + u \frac{\partial u}{\partial x} + w \frac{\partial u}{\partial z} \right) = -\frac{\partial p}{\partial x} + \varepsilon^2 \frac{\partial^2 u}{\partial x^2} + \frac{\partial^2 u}{\partial z^2}. \quad (2.21)$$

We now write (2.14), the other component of the momentum equation, in terms of dimensionless variables:

$$\rho \left(\frac{v_0^2}{d} \frac{\partial w}{\partial t} + \frac{v_0^2}{\varepsilon L} u \frac{\partial w}{\partial x} + \frac{v_0^2}{d} w \frac{\partial w}{\partial z} \right) = -\frac{p_0}{d} \frac{\partial p}{\partial z} + \mu \left(\frac{v_0}{L^2} \frac{\partial^2 w}{\partial x^2} + \frac{v_0}{d^2} \frac{\partial^2 w}{\partial z^2} \right). \quad (2.22)$$

We multiply by $d^4/L^2 (= \varepsilon^2 d^2)$:

$$\rho v_0^2 \varepsilon^2 d \left(\frac{\partial w}{\partial t} + u \frac{\partial w}{\partial x} + w \frac{\partial w}{\partial z} \right) = -p_0 \varepsilon^2 d \frac{\partial p}{\partial z} + \mu v_0 \left(\varepsilon^4 \frac{\partial^2 w}{\partial x^2} + \varepsilon^2 \frac{\partial^2 w}{\partial z^2} \right). \quad (2.23)$$

Next, we divide by μv_0 :

$$\frac{\rho v_0 \varepsilon^2 d}{\mu} \left(\frac{\partial w}{\partial t} + u \frac{\partial w}{\partial x} + w \frac{\partial w}{\partial z} \right) = -\frac{p_0 \varepsilon^2 d}{v_0 \mu} \frac{\partial p}{\partial z} + \varepsilon^4 \frac{\partial^2 w}{\partial x^2} + \varepsilon^2 \frac{\partial^2 w}{\partial z^2}. \quad (2.24)$$

Noting that $p_0 = \frac{v_0 \mu}{\varepsilon^2 d}$, the coefficient of $\frac{\partial p}{\partial z}$ simplifies greatly. Moreover, with $\text{Re} = \frac{\rho v_0 L}{\mu} = \frac{\rho v_0 d}{\varepsilon^2 \mu}$, we obtain

$$\varepsilon^4 \text{Re} \left(\frac{\partial w}{\partial t} + u \frac{\partial w}{\partial x} + w \frac{\partial w}{\partial z} \right) = -\frac{\partial p}{\partial z} + \varepsilon^4 \frac{\partial^2 w}{\partial x^2} + \varepsilon^2 \frac{\partial^2 w}{\partial z^2}. \quad (2.25)$$

We note that $\varepsilon \ll 1$ from table 2.2. Thus we can apply lubrication theory, which provides a method for simplifying thin film flows in general and for free boundary thin film problems in particular [28]. The lubrication approximation is given by expanding about ε and discarding terms beyond leading order. Applying lubrication theory to (2.17), (2.21), and (2.25), we obtain the following system of equations:

$$\frac{\partial u}{\partial x} + \frac{\partial w}{\partial z} = 0, \quad (2.26)$$

$$-\frac{\partial p}{\partial x} + \frac{\partial^2 u}{\partial z^2} = 0, \quad (2.27)$$

$$-\frac{\partial p}{\partial z} = 0. \quad (2.28)$$

2.4 Equation for Corneal Surface

We define the dimensional corneal surface to be

$$z'_c(x') = z'_a + z'_a \sin\left(\frac{2\pi x'}{\lambda'}\right), \quad (2.29)$$

where z'_a is the epithelial cell height (default $z'_a = 0.25\mu\text{m}$) and λ' is the epithelial cell width (default $\lambda' = 35\mu\text{m}$). Since z'_c and z'_a measure heights, we introduce the following dimensionless variables and parameters:

$$z_c = z'_c/d, \quad \text{and} \quad z_a = z'_a/d. \quad (2.30)$$

Moreover, we define the wavenumber to be $k = L/\lambda'$ and $x = x'/L$ based on the characteristic length scale. Then

$$dz_c(x) = dz_a + dz_a \sin(2\pi kx). \quad (2.31)$$

Dividing by d , we have that

$$z_c(x) = z_a [1 + \sin(2\pi kx)]. \quad (2.32)$$

2.5 Boundary Conditions

2.5.1 Corneal Surface

At $z' = z'_c(x')$, we have no slip boundary conditions; that is, the fluid has zero velocity relative to the boundary. Thus

$$\mathbf{u}' \cdot \mathbf{t}'_c = 0, \quad (2.33)$$

where

$$\mathbf{t}'_c = \frac{\left(1, \frac{\partial z'_c}{\partial x'}\right)}{\sqrt{1 + \left(\frac{dz'_c}{dx'}\right)^2}} \quad (2.34)$$

is the unit tangent vector to the corneal surface. Then expanding (2.33)

$$0 = \mathbf{u}' \cdot \mathbf{t}'_c = \frac{u'}{\sqrt{1 + \left(\frac{dz'_c}{dx'}\right)^2}} + \frac{w' \frac{dz'_c}{dx'}}{\sqrt{1 + \left(\frac{dz'_c}{dx'}\right)^2}} \quad (2.35)$$

$$= \frac{\frac{v_0}{\varepsilon} u}{\sqrt{1 + \varepsilon^2 \left(\frac{dz_c}{dx}\right)^2}} + \frac{v_0 w \varepsilon \frac{dz_c}{dx}}{\sqrt{1 + \varepsilon \left(\frac{dz_c}{dx}\right)^2}}. \quad (2.36)$$

Multiplying by ε , we have that

$$\frac{v_0 u + v_0 w \varepsilon^2 \frac{dz_c}{dx}}{\sqrt{1 + \varepsilon^2 \left(\frac{dz_c}{dx}\right)^2}} = 0. \quad (2.37)$$

We note that

$$\left| \frac{dz_c}{dx} \right| \leq 2\pi k z_a, \quad (2.38)$$

so $\varepsilon^2 \left(\frac{dz_c}{dx}\right)^2 = O(\varepsilon^2)$. Applying lubrication theory, we discard terms beyond leading order ε and are left with

$$v_0 u = 0 \quad \Rightarrow \quad u = 0. \quad (2.39)$$

We also have impermeability at the corneal surface. That is,

$$\mathbf{u}' \cdot \mathbf{n}'_c = 0, \quad (2.40)$$

where

$$\mathbf{n}'_c = \frac{\left(-\frac{dz'_c}{dx'}, 1\right)}{\sqrt{1 + \left(\frac{dz'_c}{dx'}\right)^2}} \quad (2.41)$$

is the unit normal vector to the corneal surface. Expanding, we have

$$0 = \mathbf{u}' \cdot \mathbf{n}'_c = \frac{-u' \frac{dz'_c}{dx'}}{\sqrt{1 + \left(\frac{dz'_c}{dx'}\right)^2}} + \frac{w'}{\sqrt{1 + \left(\frac{dz'_c}{dx'}\right)^2}} \quad (2.42)$$

$$= \frac{-\frac{v_0}{\varepsilon} u \varepsilon \frac{dz_c}{dx}}{\sqrt{1 + \varepsilon^2 \left(\frac{dz'_c}{dx'}\right)^2}} + \frac{v_0 w}{\sqrt{1 + \varepsilon^2 \left(\frac{dz'_c}{dx'}\right)^2}}. \quad (2.43)$$

Dropping terms of order ε^2 or higher, we are left with

$$v_0 \left(u \frac{\partial z_c}{\partial x} + w \right) = 0. \quad (2.44)$$

But we have already found that $u = 0$ at $z = z_c(x)$ from (2.39). Then dividing by v_0 , we obtain a dimensionless impermeability condition of

$$w = 0. \quad (2.45)$$

From 2.39 and 2.45 we have that there is no movement of the fluid at the corneal surface.

2.5.2 Free Surface

Let $h'(x', t')$ be the thickness of the aqueous layer at width x' and time t' . Then we define

$$H'(x', t') = h'(x', t') + z'_c(x') \quad (2.46)$$

to be the dimensional equation describing the position/height of the fluid-air interface, or free surface of the tear film. At $z' = H'(x', t')$, we must satisfy the following conditions: tangential immobility, kinematic condition, and normal stress balance. We introduce the dimensionless variables

$$h = h'/d, \quad H = H'/d, \quad J = J'/(\rho v_0), \quad \text{and} \quad \Pi = \Pi'/p_0, \quad (2.47)$$

where

$$\Pi' = \frac{A^*}{6\pi} h'^{-3} \quad (2.48)$$

represents the van der Waals' wetting forces [27]. In chapter 4 we vary Π , using (2.48) as the default. We derive dimensionless equations for each of the boundary conditions below. Typical parameter values can be found in table 2.1.

Tangential Immobility

First, we consider tangential immobility; that is,

$$\mathbf{u}' \cdot \mathbf{t}' = 0 \quad (2.49)$$

where

$$\mathbf{t}' = \frac{(1, \frac{\partial H'}{\partial x'})}{\sqrt{1 + (\frac{\partial H'}{\partial x'})^2}} \quad (2.50)$$

is the unit tangent vector of the free surface. We compute the dot product in (2.49) to obtain

$$\frac{u'}{\sqrt{1 + (\frac{\partial H'}{\partial x'})^2}} + \frac{w' \frac{\partial H'}{\partial x'}}{\sqrt{1 + (\frac{\partial H'}{\partial x'})^2}} = 0. \quad (2.51)$$

Nondimensionalizing, we have that

$$\frac{\frac{v_0}{\varepsilon} u}{\sqrt{1 + \varepsilon^2 (\frac{\partial H'}{\partial x'})^2}} + \frac{v_0 w \varepsilon \frac{\partial H}{\partial x}}{\sqrt{1 + \varepsilon^2 (\frac{\partial H'}{\partial x'})^2}} = 0. \quad (2.52)$$

We multiply (2.52) by ε/v_0 :

$$\frac{u}{\sqrt{1 + \varepsilon^2 (\frac{\partial H'}{\partial x'})^2}} + \frac{\varepsilon^2 w \frac{\partial H}{\partial x}}{\sqrt{1 + \varepsilon^2 (\frac{\partial H'}{\partial x'})^2}} = 0. \quad (2.53)$$

Discarding terms of order ε^2 or greater (from lubrication theory), we obtain

$$u = 0. \quad (2.54)$$

Kinematic Condition

The kinematic condition conserves mass at the free surface. We begin with the dimensional mass balance equation, as given in [27]:

$$\rho(\mathbf{u}' - \mathbf{u}'_1) \cdot \mathbf{n}' = J' \quad (2.55)$$

where

$$\mathbf{u}' = \left(0, \frac{\partial H'}{\partial t'} \right) \quad (2.56)$$

is the interface velocity at the free surface, $J'(x')$ is the dimensional evaporation function given by

$$J'(x') = \rho v_1 + \rho (v_0 - v_1) \exp \left[\left(-\frac{x' - x_L/2}{x_w} \right)^2 / 2 \right], \quad (2.57)$$

and

$$\mathbf{n}' = \frac{\left(-\frac{\partial H'}{\partial x'}, 1 \right)}{\sqrt{1 + \frac{\partial H'^2}{\partial x'^2}}} \quad (2.58)$$

is the outward unit normal at the free surface. In (2.57), $x_w = 1.2$ is the typical evaporation width that we use, $x_L = 8$ is the domain length, and typical values for ρ , v_0 , and v_1 are found in table 2.1. From (2.58), we have that (2.55) becomes

$$\rho \left(u', v' - \frac{\partial H'}{\partial t'} \right) \cdot \left(-\frac{\partial H'}{\partial x'}, 1 \right) = J' \sqrt{1 + \left(\frac{\partial H'}{\partial x'} \right)^2}. \quad (2.59)$$

Expanding the dot product, we have

$$\rho \left(-\frac{\partial H'}{\partial x'} u' + v' - \frac{\partial H'}{\partial t'} \right) = J' \sqrt{1 + \left(\frac{\partial H'}{\partial x'} \right)^2}. \quad (2.60)$$

Given that $H' = h' + z'_c$, we have that

$$\rho \left(-\frac{\partial h'}{\partial x'} u' - \frac{dz'_c}{dx'} u' + v' - \frac{\partial h'}{\partial t'} \right) = J' \sqrt{1 + \left(\frac{\partial h'}{\partial x'} + \frac{dz'_c}{dx'} \right)^2}. \quad (2.61)$$

We now nondimensionalize:

$$\rho \left(-\frac{d}{L} \frac{v_0}{\varepsilon} \frac{\partial h}{\partial x} u - \frac{d}{L} \frac{v_0}{\varepsilon} \frac{dz_c}{dx} u + v_0 w - \frac{dv_0}{d} \frac{\partial h}{\partial t} \right) = \rho v_0 J \sqrt{1 + \left(\frac{d}{L} \frac{\partial h}{\partial x} + \frac{d}{L} \frac{dz_c}{dx} \right)^2}. \quad (2.62)$$

Given that $\varepsilon = d/L$, we discard terms beyond leading order and obtain

$$\rho v_0 \left(-\frac{\partial h}{\partial x} u - \frac{dz_c}{dx} u + w - \frac{\partial h}{\partial t} \right) = \rho v_0 J. \quad (2.63)$$

Dividing by ρv_0 and using that $H = h + z_c$, we have that at $z = H(x, t)$,

$$w = J + u \frac{\partial H}{\partial x} + \frac{\partial H}{\partial t}. \quad (2.64)$$

Normal Stress Balance

We begin with the normal stress balance

$$-p'_v - \mathbf{n}' \cdot \mathbf{T}' \cdot \mathbf{n}' = \sigma_0 \nabla' \cdot \mathbf{n}' - \Pi'(h') \quad (2.65)$$

where

$$\mathbf{T}' = -p' \mathbf{I} + \mu [\nabla' \mathbf{u}' + (\nabla' \mathbf{u}')^T] \quad (2.66)$$

is the Newtonian stress tensor and σ_0 is the surface tension constant. Enumerating the vectors and stress tensor, we obtain

$$\begin{aligned} -p'_v - \frac{\left(-\frac{\partial H'}{\partial x'}, 1\right)}{1 + \left(\frac{\partial H'}{\partial x'}\right)^2} \begin{pmatrix} -p' + 2\mu \frac{\partial u'}{\partial x'} & \frac{\partial w'}{\partial x'} + \frac{\partial u'}{\partial z'} \\ \frac{\partial w'}{\partial x'} + \frac{\partial u'}{\partial z'} & -p' + 2\mu \frac{\partial w'}{\partial z'} \end{pmatrix} \begin{pmatrix} -\frac{\partial H'}{\partial x'} \\ 1 \end{pmatrix} \\ = \sigma_0 \left(\frac{\partial}{\partial x'}, \frac{\partial}{\partial z'} \right) \cdot \begin{pmatrix} \frac{-\frac{\partial H'}{\partial x'}}{\sqrt{1 + \left(\frac{\partial H'}{\partial x'}\right)^2}} \\ \frac{1}{\sqrt{1 + \left(\frac{\partial H'}{\partial x'}\right)^2}} \end{pmatrix} - \Pi'(h'). \end{aligned} \quad (2.67)$$

Now we perform the matrix and vector multiplications to obtain the following equation:

$$\begin{aligned} -p'_v - \frac{1}{1 + \left(\frac{\partial H'}{\partial x'}\right)^2} \left[\left(-1 - \left(\frac{\partial H'}{\partial x'}\right)^2\right) p' - 2\mu \frac{\partial u'}{\partial x'} \left(\frac{\partial H'}{\partial x'}\right)^2 - 2 \frac{\partial w'}{\partial x'} \frac{\partial H'}{\partial x'} - 2 \frac{\partial u'}{\partial z'} \frac{\partial H'}{\partial x'} + 2\mu \frac{\partial w'}{\partial z'} \right] \\ = \frac{\sigma_0}{1 + \left(\frac{\partial H'}{\partial x'}\right)^2} \left(-\sqrt{1 + \left(\frac{\partial H'}{\partial x'}\right)^2} \frac{\partial^2 H'}{\partial x'^2} + \frac{\partial H'^2}{\partial x'} \frac{\partial^2 H'}{\partial x'^2} \frac{1}{\sqrt{1 + \left(\frac{\partial H'}{\partial x'}\right)^2}} \right) - \Pi'(h'). \end{aligned} \quad (2.68)$$

We expand the term involving p' to obtain

$$\begin{aligned} -p'_v + p' - \frac{2}{1 + \left(\frac{\partial H'}{\partial x'}\right)^2} \left(-\mu \frac{\partial u'}{\partial x'} \left(\frac{\partial H'}{\partial x'}\right)^2 - \frac{\partial w'}{\partial x'} \frac{\partial H'}{\partial x'} - \frac{\partial u'}{\partial z'} \frac{\partial H'}{\partial x'} + \mu \frac{\partial w'}{\partial z'} \right) \\ = \frac{-\sigma_0 \frac{\partial^2 H'}{\partial x'^2}}{\left(1 + \left(\frac{\partial H'}{\partial x'}\right)^2\right)^{3/2}} - \Pi'(h'). \end{aligned} \quad (2.69)$$

We now nondimensionalize:

$$\begin{aligned} \frac{-v_0\mu}{\varepsilon^2 d} p - \frac{2}{1 + \left(\varepsilon \frac{\partial H}{\partial x}\right)^2} \left(-\mu\varepsilon \left(\frac{\partial H}{\partial x}\right)^2 \frac{v_0}{L} \frac{\partial u}{\partial x} - \frac{\varepsilon v_0}{L} \frac{\partial H}{\partial x} \frac{\partial w}{\partial x} - \frac{v_0}{d} \frac{\partial H}{\partial x} \frac{\partial u}{\partial z} + \frac{\mu v_0}{d} \frac{\partial w}{\partial z} \right) \\ = -\frac{\sigma_0 \varepsilon}{L} \frac{\frac{\partial^2 H}{\partial x^2}}{\left(1 + \varepsilon^2 \left(\frac{\partial H}{\partial x}\right)^2\right)^{3/2}} - \frac{v_0 \mu}{\varepsilon^2 d} \Pi(h). \end{aligned} \quad (2.70)$$

We divide by $\frac{v_0\mu}{\varepsilon^2 d}$:

$$p - \frac{2}{1 + \left(\varepsilon \frac{\partial H}{\partial x}\right)^2} \left(-\varepsilon^4 \left(\frac{\partial H}{\partial x}\right)^2 \frac{\partial u}{\partial x} - \frac{1}{\mu} \varepsilon^4 \frac{\partial H}{\partial x} \frac{\partial w}{\partial x} - \frac{1}{\mu} \varepsilon^2 \frac{\partial H}{\partial x} \frac{\partial u}{\partial z} \right) \quad (2.71)$$

$$= -\frac{\sigma_0 \varepsilon^4}{v_0 \mu} \frac{\frac{\partial^2 H}{\partial x^2}}{\left(1 + \varepsilon^2 \left(\frac{\partial H}{\partial x}\right)^2\right)^{3/2}} - \Pi(h). \quad (2.72)$$

Since the domain length L is given by (2.2), then we obtain that

$$\varepsilon^4 = \frac{v_0 \mu}{\sigma_0}. \quad (2.73)$$

Substituting this expression for ε^4 , we obtain

$$\begin{aligned} p - \frac{2}{1 + \left(\varepsilon \frac{\partial H}{\partial x}\right)^2} \left(-\varepsilon^4 \left(\frac{\partial H}{\partial x}\right)^2 \frac{\partial u}{\partial x} - \frac{1}{\mu} \varepsilon^4 \frac{\partial H}{\partial x} \frac{\partial w}{\partial x} - \frac{1}{\mu} \varepsilon^2 \frac{\partial H}{\partial x} \frac{\partial u}{\partial z} \right) \\ = \frac{-\frac{\partial^2 H}{\partial x^2}}{\left(1 + \varepsilon^2 \left(\frac{\partial H}{\partial x}\right)^2\right)^{3/2}} - \Pi(h). \end{aligned} \quad (2.74)$$

Now applying lubrication theory, given $\varepsilon \ll 1$, we discard terms of order ε^2 or higher.

Then the equation simplifies to

$$p = -\frac{\partial^2 H}{\partial x^2} - \Pi(h). \quad (2.75)$$

2.6 Governing Equations in Thin Film Limit

We summarize the equations we have derived.

Interior

In $z_c(x) < z < h(x, t) + z_c(x)$, we have

$$\frac{\partial u}{\partial x} + \frac{\partial w}{\partial z} = 0, \quad (2.76)$$

$$-\frac{\partial p}{\partial x} + \frac{\partial^2 u}{\partial z^2} = 0, \quad (2.77)$$

$$-\frac{\partial p}{\partial z} = 0. \quad (2.78)$$

Corneal Surface

On $z = z_c(x)$, we obtained

$$u = 0, \quad (2.79)$$

$$w = 0. \quad (2.80)$$

Free Surface

On $z = h(x, t) + z_c(x)$, we have

$$u = 0, \quad (2.81)$$

$$w = \frac{\partial h}{\partial t} + u \left(\frac{\partial h}{\partial x} + \frac{dz_c}{dx} \right) + J, \quad (2.82)$$

$$p = -\frac{\partial^2 h}{\partial x^2} - \frac{d^2 z_c}{dx^2} - \Pi(h). \quad (2.83)$$

2.7 Reduction

With a lubrication approximation, we will reduce the above system of free boundary PDEs to a single PDE for the thickness of the aqueous layer. From (2.83), and (2.78), we obtain that

$$p = p(x). \quad (2.84)$$

Now we combine (2.84) with (2.77) and integrate twice, using dummy variables as placeholders for z :

$$0 = \int^z \int^s \left[-\frac{\partial p}{\partial x} + \frac{\partial^2 u}{\partial r^2} \right] dr ds \quad (2.85)$$

$$= \int^z \left[-\frac{\partial p}{\partial x} s + \frac{\partial u}{\partial s} - c_1 \right] ds \quad (2.86)$$

$$= -\frac{1}{2} \frac{\partial p}{\partial x} z^2 + u - c_1 z - c_2. \quad (2.87)$$

Rearranging terms in (2.87), we obtain the following equation for u :

$$u = \frac{1}{2} \frac{\partial p}{\partial x} z^2 + c_1 z + c_2. \quad (2.88)$$

We now apply the boundary conditions to solve for c_1 and c_2 : At the corneal surface, we have

$$u(x, z_c, t) = \frac{1}{2} \frac{\partial p}{\partial x} z_c(x)^2 + c_1 z_c(x) + c_2, \quad (2.89)$$

and at the free surface,

$$u(x, h + z_c, t) = \frac{1}{2} \frac{\partial p}{\partial x} [h(x, t) + z_c(x)]^2 + c_1 [h(x, t) + z_c(x)] + c_2. \quad (2.90)$$

We subtract (2.89) from (2.90) to obtain

$$u(x, h + z_c, t) - u(x, z_c, t) = \frac{1}{2} \frac{\partial p}{\partial x} [h^2(x, t) + 2h(x, t)z_c(x)] + c_1 h(x, t). \quad (2.91)$$

But we note from (2.79) and (2.81) that $u = 0$ on the corneal surface and the free surface, so the left-hand side is equal to zero and we obtain that

$$c_1 = -\frac{1}{2} \frac{\partial p}{\partial x} [h(x, t) + 2z_c(x)]. \quad (2.92)$$

Now we substitute the given value of c_1 into (2.89) in order to find c_2 :

$$\frac{1}{2} \frac{\partial p}{\partial x} z_c(x)^2 - \frac{1}{2} \frac{\partial p}{\partial x} [h(x, t) + 2z_c(x)] z_c(x) + c_2 = 0, \quad (2.93)$$

so that

$$c_2 = \frac{1}{2} \frac{\partial p}{\partial x} [h(x, t)z_c(x) + z_c^2(x)]. \quad (2.94)$$

Substituting c_1 and c_2 into (2.88), we have

$$u(x, z, t) = \frac{1}{2} \frac{\partial p}{\partial x} \{z^2 - [h(x, t) + 2z_c(x)]z + h(x, t)z_c(x) + z_c(x)^2\}. \quad (2.95)$$

Next we integrate (2.76) along our domain with respect to z :

$$\int_{z_c}^H \left(\frac{\partial u}{\partial x} + \frac{\partial w}{\partial z} \right) dz = 0; \quad (2.96)$$

$$w(H) - w(z_c) + \int_{z_c}^H \frac{\partial u}{\partial x} dz = 0; \quad (2.97)$$

$$w(H) + \int_{z_c}^H \frac{\partial u}{\partial x} dz = 0. \quad (2.98)$$

From (2.82), we have that

$$w(H) = \frac{\partial H}{\partial t} + u(H) \frac{\partial H}{\partial x} + J. \quad (2.99)$$

Substituting this value for $w(H)$, we obtain

$$\frac{\partial H}{\partial t} + u(H) \frac{\partial H}{\partial x} + \int_{z_c}^H \frac{\partial u}{\partial x} dz = -J. \quad (2.100)$$

Next we apply the Leibniz integral rule, which states that given a function f with continuous partial derivative with respect to t , then

$$\frac{d}{dt} \left(\int_{a(t)}^{b(t)} f(x, t) dx \right) = \int_{a(t)}^{b(t)} \frac{\partial f}{\partial t} dx + f(b(t), t) \frac{db}{dt} - f(a(t), t) \frac{da}{dt}. \quad (2.101)$$

Applying (2.101) to (2.100), we have

$$\frac{\partial H}{\partial t} + u(H) \frac{\partial H}{\partial x} + \frac{\partial}{\partial x} \int_{z_c}^H u dz + u(z_c) \frac{\partial z_c}{\partial x} - u(H) \frac{\partial H}{\partial x} = -J. \quad (2.102)$$

Given the no slip boundary condition (2.79) on the corneal surface, we are left with

$$-J = \frac{\partial H}{\partial t} + \frac{\partial}{\partial x} \int_{z_c}^H u dz. \quad (2.103)$$

Now we substitute for u and integrate with respect to z :

$$-J = \frac{\partial H}{\partial t} + \frac{\partial}{\partial x} \int_{z_c}^H \frac{1}{2} \frac{\partial p}{\partial x} (z^2 - (h + 2z_c)z + hz_c + z_c^2) dz \quad (2.104)$$

$$= \frac{\partial H}{\partial t} + \frac{\partial}{\partial x} \left\{ \frac{1}{2} \frac{\partial p}{\partial x} \left[\frac{1}{3} z^3 - \frac{1}{2} (h + 2z_c) z^2 + (hz_c + z_c^2) z \right] \right\} \Big|_{z_c}^H \quad (2.105)$$

$$= \frac{\partial H}{\partial t} + \frac{\partial}{\partial x} \left\{ \frac{1}{2} \frac{\partial p}{\partial x} \left[\frac{1}{3} (H^3 - z_c^3) - \frac{1}{2} (h + 2z_c) (H^2 - z_c^2) + (hz_c + z_c^2) (H - z_c) \right] \right\}. \quad (2.106)$$

After expanding and canceling terms, we are left with

$$\frac{\partial H}{\partial t} + \frac{1}{2} \frac{\partial}{\partial x} \left(-\frac{1}{6} \frac{\partial p}{\partial x} h^3 \right) = -J. \quad (2.107)$$

Since $H = h + z_c$ and $z_c = z_c(x)$, then $\frac{\partial H}{\partial t} = \frac{\partial h}{\partial t}$ and the PDEs we are left to solve are

$$\frac{\partial h}{\partial t} - \frac{1}{12} \frac{\partial}{\partial x} \left(h^3 \frac{\partial p}{\partial x} \right) = -J, \quad (2.108)$$

$$p = -\frac{\partial^2 h}{\partial x^2} - \frac{d^2 z_c}{dx^2} - \Pi(h), \quad (2.109)$$

where

$$J(x) = \frac{v_1}{v_0} + \left(1 - \frac{v_1}{v_0} \right) \cdot \exp \left(\frac{-(x - \frac{x_L}{2})^2}{2x_w^2} \right), \quad (2.110)$$

$$z_c(x) = z_a [1 + \sin(2\pi kx)], \quad (2.111)$$

$$\Pi(h) = Ah^{-3}, \quad (2.112)$$

$$0 \leq x \leq x_L, \quad t \geq 0. \quad (2.113)$$

We impose flat initial conditions:

$$h(x, 0) = 1 - z_c(x) - z_a, \quad (2.114)$$

$$p(x, 0) = -\Pi(h(x, 0)). \quad (2.115)$$

Chapter 3

NUMERICAL DISCRETIZATION

The PDE we derived in the previous section is nonlinear first order in time and fourth order in space, which contributes to its lack of a closed form analytical solution. Therefore, we turn to numerical methods for approximating a solution. We first discretize spatially, to obtain a system of differential-algebraic equations (DAE). Then we solve the DAE system in Matlab [29]. In this chapter, we explain the process by which we discretize and approximate the PDE solution.

We recall that the problem is defined on a localized region of the eye, with characteristic length scale of about 350 microns. At such a length scale, we have the liberty of modeling a localized region of particular interest. We consider a section of the eye that does not share a boundary with the eyelid, perhaps the center of the eye. This allows us to enforce periodic boundary conditions at $x = 0$ and $x = x_L$. That is, $h(0, t) = h(x_L, t)$ for all t . With periodic boundary conditions, we can apply Fourier spectral methods for spatial discretization. We apply Fourier spectral methods using differentiation matrices as derived by [30], and due to periodicity we do not impose a separate case for boundary conditions. We choose the number of gridpoints to be

$$N = 10x_L k \tag{3.1}$$

to ensure that the grid captures the intricacies of the ocular surface. The gridpoints x_i are evenly spaced and given as

$$x_i = \frac{x_L}{N}i = \frac{1}{10k}i, \quad \text{for } i = 1, \dots, N. \tag{3.2}$$

Numerical testing on the second derivative d^2z_c/dx^2 ensures that we obtain accurate derivatives with such grid spacing.

Applying Fourier spectral methods in space, we obtain discrete variables for p , h , and z_c as defined below:

$$h_i(t) = h(x_i, t), \quad p_i(t) = p(x_i, t), \quad \text{and } z_{c_i} = z_c(x_i) \quad \text{for } i = 1, \dots, N. \quad (3.3)$$

Then the PDE reduces to a system of DAEs:

$$\frac{\partial h_i}{\partial t} = f(p_i(t), h_i(t)), \quad (3.4)$$

$$0 = g(p_i(t), h_i(t), z_{c_i}), \quad (3.5)$$

with initial conditions

$$h_i(0) = 1 - z_a - z_{c_i}, \quad (3.6)$$

$$p_i(0) = -\Pi(h_i(0)). \quad (3.7)$$

Note that (3.6) ensures a flat initial condition, for a tear film of characteristic thickness. Given this DAE system, we use Matlab's built-in `ode15s` solver to find an approximate numerical solution [29]. This is a stiff solver which we choose due to the varying rates of decay from the fourth order spatial derivative and first order time derivative [31]. When running `ode15s`, we implement a stopping criterion based on a minimum thickness of h . In our results, we predominantly use two different stopping criteria. One case is when the tear film stops as it reaches the glycocalyx. In that case, we stop when $\min_{x'} h'(x', t') = 0.25\mu\text{m}$ dimensionally, or $\min_x h(x, t) = 1/14$. We employ this case when studying the effect of ocular surface features on tear film dynamics. In other instances, when we explore the effect of conjoining pressures for the film at low thicknesses, we use the stopping criterion $\min_{x'} h'(x', t') = 0.035\mu\text{m}$ dimensionally, or $\min_x h(x, t) = 10^{-2}$. Given the height of the glycocalyx of $0.2-0.5\mu\text{m}$ [4], this stopping criterion implies that the aqueous layer can thin below the glycocalyx.

Due to evidence that the glycocalyx helps maintain the aqueous layer covering of the corneal surface [32], thinning of the film in the model may be have implications of a dysfunctional glycocalyx or that there is some compliance of the glycocalyx.

Chapter 4

RESULTS

In the first section, we study the tear film dynamics at TBU by varying the parameters of the corneal surface function and use a stopping criterion of $\min_x h(x, t) = 1/14$. In the second section, we explore the tear film dynamics at TBU with different functions for conjoining pressure and wetting forces, which create a repulsive force between the free surface and ocular surface, and use a stopping criterion of $\min_x h(x, t) = 0.01$.

4.1 Effect of Corneal Surface Features

By introducing a sinusoidal function at the boundary between the tear film and the ocular surface, we observe different tear film dynamics than in the case of a flat tear film/ocular surface boundary. Figure 4.1 compares and contrasts the model with a rough (sinusoidal) corneal surface on the left and flat corneal surface on the right. The initial conditions in each plot are $h(x, 0) = 1 - z_c(x) - z_a$. In the rough case, $z_c(x)$ is given by (2.32) and $z_a = 1/14$ (dimensionless amplitude). For the flat ocular surface, $z_c(x) = 0$ and $z_a = 0$. We observe the same qualitative behavior in the plots of the first four displayed time values, while the tear film is thinning before it reaches TBU. However, at the final timestep, we observe different behavior in each model. In the model with the rough corneal surface, the tear film has ripples at the region of TBU. In the smooth corneal surface model, TBU occurs but with no wrinkling of the tear film. The contrasting plots of figure 4.1 illustrate the importance of the ocular surface in determining tear film dynamics at TBU. We now focus our attention on the case of a rough corneal surface, and study how variations in the surface influence tear film dynamics.

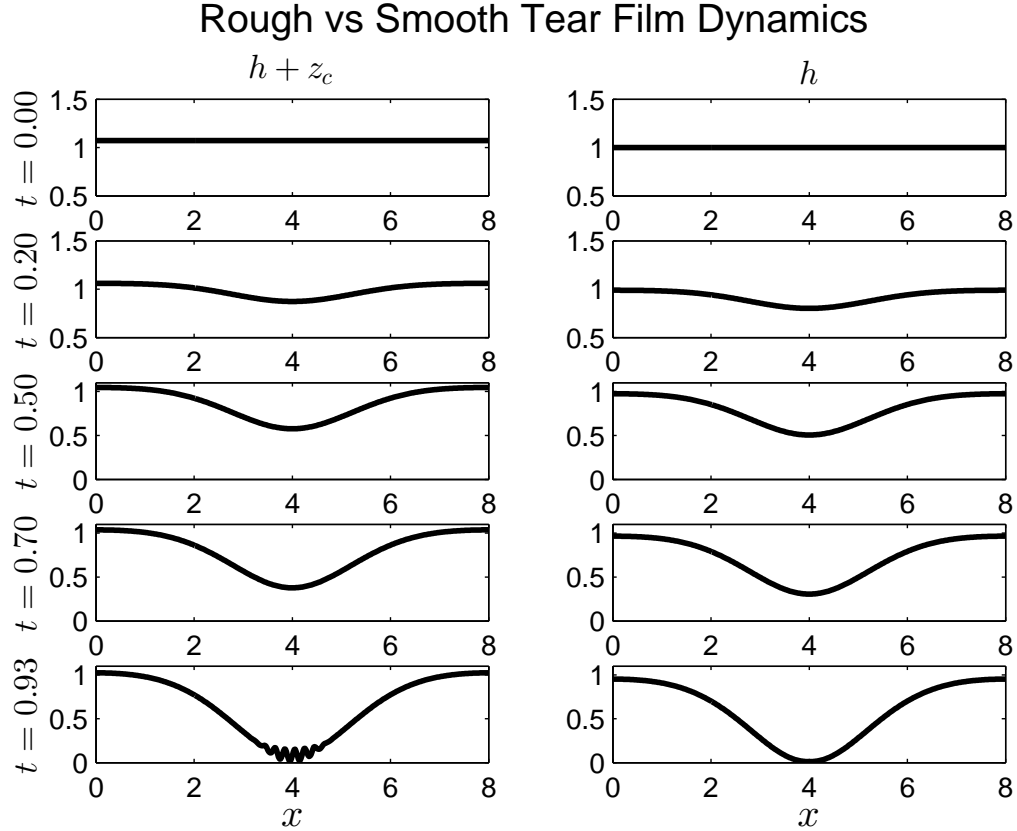


Figure 4.1: Time series plots of aqueous layer thickness with sinusoidal corneal surface (left) vs. flat corneal surface (right). The model exhibits the same behavior up until time $t = t_{\text{end}}$ (dimensionless 1.07; dimensional 11.24s), at which time the film anterior to the rough surface develops ripples at TBU. The film anterior to the flat corneal surface also reaches TBU, but with no ripples.

Effect of Wavenumber on Roughness

Our model uses a default wavenumber of 10 (i.e. 10 periods per unit length), based on the average experimental epithelial cell width [6]. This number is merely an

average, and experimental studies have observed great variability in corneal surface features among human subjects [5, 7]. The corneal epithelium continuously undergoes changes, losing cells to cell death and gaining new cells through cell division [33]. We incorporate such biological processes into our model by varying the wavenumber. For example, a wavenumber less than 10 may represent clumping of cells due to epithelial erosion, and a wavenumber greater than 10 reflects smaller cells created during cell division, along with intracellular variation [33]. In model simulations with different wavenumbers, we observe fewer and deeper grooves with lower wavenumber, and a flatter tear film comprising shallower grooves with a higher wavenumber; see figure 4.2 for a comparison.

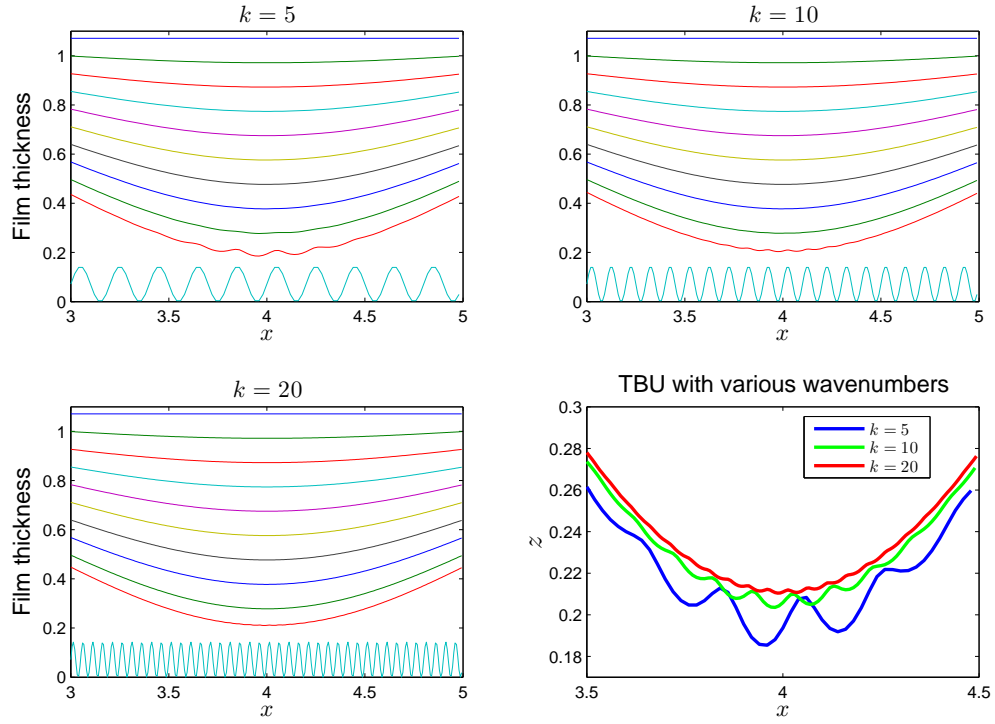


Figure 4.2: Comparison of tear film dynamics with varying corneal surface wavenumber. The first three subplots contain numerical results for $k = 5$, $k = 10$, and $k = 20$, respectively, with the corneal surface plotted at the bottom of each figure in blue. Solution curves represent the location of the free surface at each time step. Time starts at $t = 0$, increasing by 0.1 until final time $t = 0.8821$. As t increases, $h + z_c$ decreases monotonically. The final figure compares the tear film at TBU with each wavenumber.

Figure 4.2 gives us a preliminary notion of the effect of wavenumber on tear film rippling. With such intuition, we aim to quantify the variation in the rippling by

computing an approximate amplitude of the tear film; refer to figure 4.3 for a sketch of the procedure.

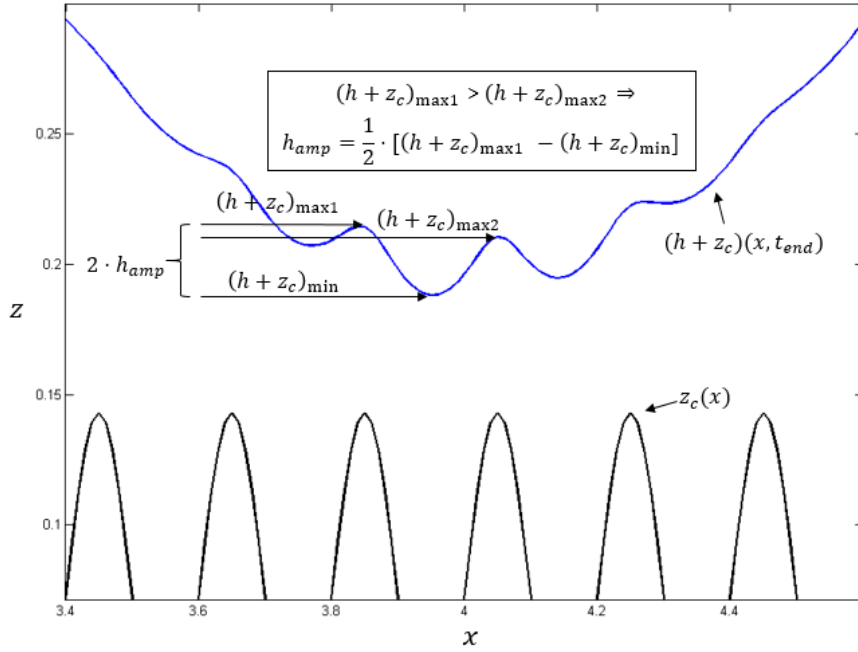


Figure 4.3: Procedure for finding the approximate tear film amplitude.

We begin by numerically finding the absolute minimum of $h + z_c$ where TBU occurs, and then finding the local maxima adjacent to this minimum. We choose the larger of the maxima, and then compute the difference from peak to valley, dividing by 2 for consistency with a sinusoidal amplitude. We call this quantity h_{amp} , the tear film amplitude. Next we compute the ratio of tear film amplitude to corneal surface amplitude z_a , $r = h_{amp}/z_a$ and plot this ratio r versus the wavenumber k . Note that we use integer wavenumbers to ensure periodicity for a given domain length, which is required for use of Fourier spectral methods. Figure 4.4 displays the ratio versus wavenumber.

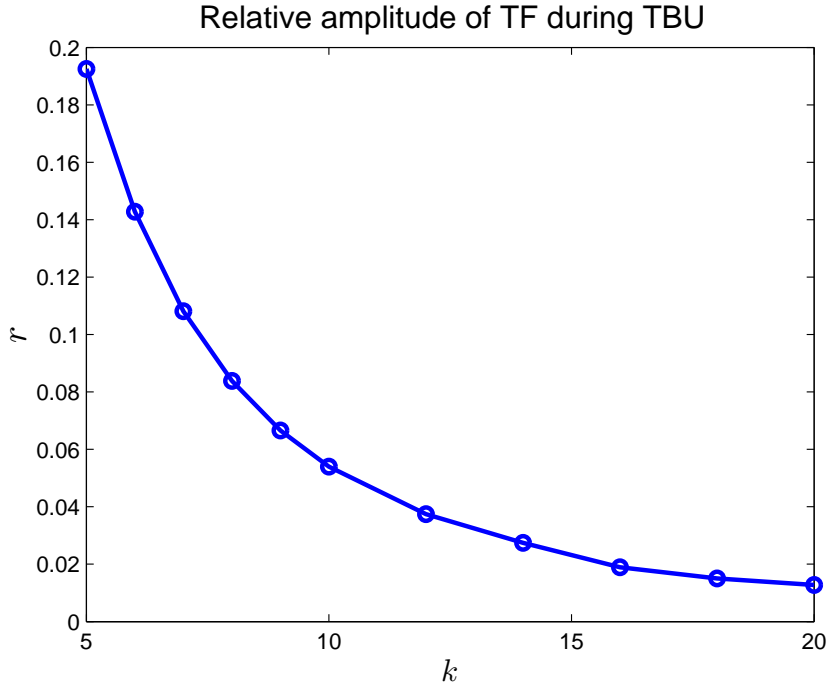


Figure 4.4: Ratio of the tear film amplitude to the corneal surface amplitude as a function of corneal surface wavenumber. Tear film roughness decreases as the wavenumber increases. At the default wavenumber $k = 10$, the ratio is less than 0.06. At $k = 5$, the TBU tear film amplitude to corneal surface amplitude is its highest at almost 0.2.

Quadratic Fit of Wavelength Variation

Based on the results of figure 4.4, we attempted to fit a polynomial to the data but that did not yield a strong fit. In attempt to find a better fit, we made a change of independent variable to model the ratios as a function of dimensionless wavelength $\lambda = \frac{\lambda'}{L} = \frac{1}{k}$. Making such change of variables gives the ratio as an increasing function of wavelength, rather than the decreasing behavior of figure 4.4. We use Matlab's `polyfit` function, which yields a best fit in terms of least squares, to fit the model values to a quadratic polynomial. We obtain the following polynomial to estimate r :

$$\hat{r} = 3.3122\lambda^2 + 0.3957\lambda - 0.0175, \quad (4.1)$$

where \hat{r} is the approximated ratio of tear film amplitude to ocular surface amplitude, and λ is the dimensionless wavelength. Figure 4.5 shows the values computed from the thin film model (circles) and the polynomial fit (curve).

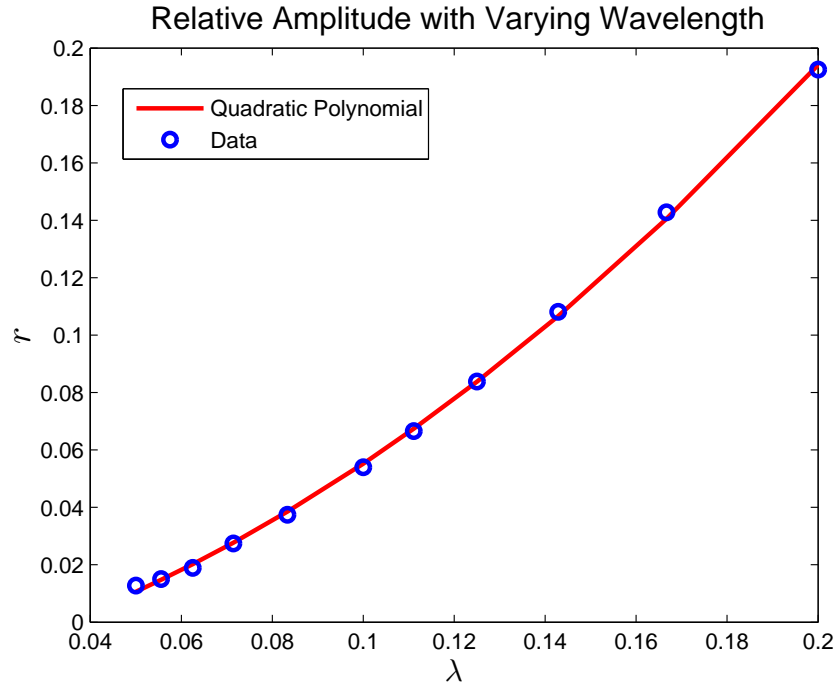


Figure 4.5: Quadratic polynomial fit, given by (4.1) (red curve) plotted with simulation data for the wavelengths corresponding to integer wavenumbers (blue circles).

Using (4.1), we obtain a good fit for the dimensionless wavelength values of interest, which vary from $\lambda = 0.05$ to $\lambda = 0.2$. The polynomial fit has residual sum of squares

$$RSS = \sum_{i=1}^{\text{length}(r)} (r_i - \hat{r}_i)^2 = 1.983 \times 10^{-5}. \quad (4.2)$$

The smallest wavelength 0.05, at the left of the plot, corresponds to wavenumber $k = 20$, where the tear film only exhibits about 1% the amplitude of the corneal surface. The largest wavelength 0.2 corresponds to wavenumber $k = 5$, where the tear film exhibits almost 20% the roughness of the corneal surface.

Effect of Amplitude on Roughness

Equation (2.32) for the corneal surface is governed by two parameters: wavenumber and amplitude. In the previous section, we established a quadratic dependence of tear film roughness on the wavelength of the corneal surface. The biological processes outlined in the previous section may also have an effect on ocular surface amplitude, e.g. an increased amplitude due to gaps formed by epithelial erosion. In this section, we explore the effect of the corneal surface amplitude on the tear film roughness, with several cases based on different fixed wavenumbers. We calculate the tear film roughness using the same procedure as before, this time normalizing with the appropriate ocular surface amplitude for each simulation. First, we consider the case when $k = 10$ (default wavenumber). Using linear least squares, we find that the model values are nearly proportional to $1/z_a$, with log-log slope -0.9912 . We use a nonlinear curve fitting tool in Matlab to find the curve of best fit

$$\hat{r} = .0038 + \frac{.0034}{z_a}. \quad (4.3)$$

The error is given by

$$RSS = \sum_{i=1}^{\text{length}(r)} (r_i - \hat{r}_i)^2 = 7.3458 \times 10^{-5}. \quad (4.4)$$

Figure 4.6 displays the curve along with the simulation values.

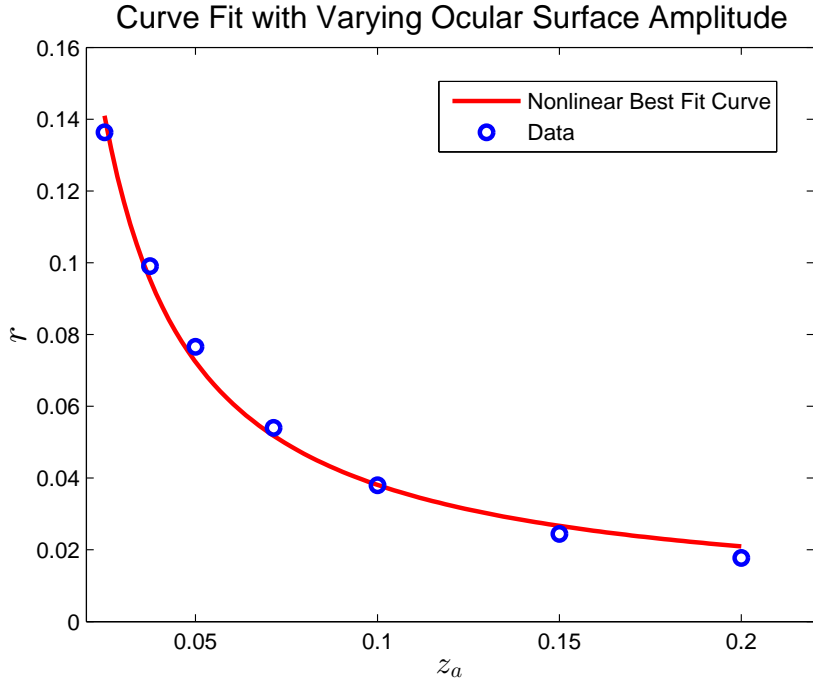


Figure 4.6: Nonlinear curve fit of the ratio values plotted as the red line, with the ratio values plotted as blue circles.

We observe from figure 4.6 that the relative roughness r decreases as we increase the ocular surface amplitude, with the highest value of r occurring when $z_a = 0.025$. Since $r = h_{amp}/z_a$, both numerator and denominator vary in the case of varying corneal surface amplitude. For lower values of z_a , we note that h_{amp} need not be as large as in the case of higher values of z_a to obtain a large value of r . We therefore explore whether the largest r and largest h_{amp} correspond to the same value of z_a . The results for h_{amp} with varying z_a are displayed in figure 4.7.

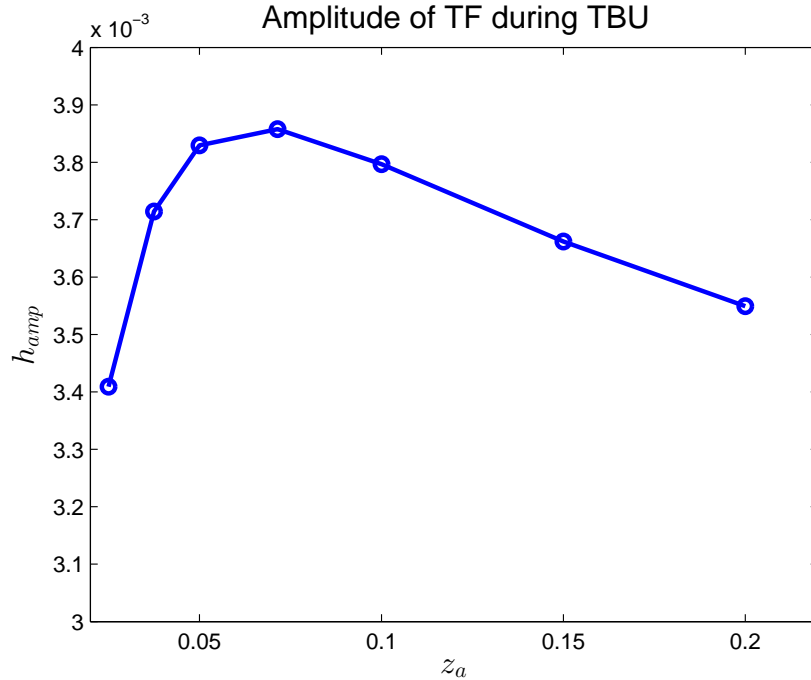


Figure 4.7: Amplitude of the tear film versus the amplitude of the corneal surface when $k = 10$. We obtain the largest amplitude for the default ocular surface amplitude $z_a = 1/14$, contrasting with the relative amplitude case in which the largest r value occurred at $z_a = 0.025$.

When we varied wavenumber in the previous section, we found the largest tear film amplitude when $k = 5$. For this wavenumber, we vary the ocular surface amplitude and calculate the relative amplitude r and dimensionless amplitude h_{amp} of the tear film at TBU. Figures 4.8 and 4.9 display the results. In both the $k = 10$ and $k = 5$ cases, we find that r is a monotonically decreasing function of z_a , and can reasonably approximate the relationship with a function of the form $r = c_1 + c_2/z_a$. When calculating h_{amp} , however, we find that the largest value of h_{amp} shifts from occurring at $z_a = 1/14$ for $k = 10$ to $z_a = 3/20$ for $k = 5$. Commensurate with the results on varying wavenumber, we obtain higher values of roughness when $k = 5$ than when $k = 10$ for varying z_a . We

use the same procedure to find the log-log slope of r versus z_a for $k = 5$ as in the case with $k = 10$, to find a log-log slope of -0.8613 . Although we do not expect as accurate a fit since this slope is further from -1 , we fit to a function of the form $c_1 + c_2/z_a$. We find the curve of best fit

$$\hat{r} = .0404 + \frac{.0098}{z_a}. \quad (4.5)$$

The error is given by

$$RSS = \sum_{i=1}^{\text{length}(r)} (r_i - \hat{r}_i)^2 = 1.9 \times 10^{-3}. \quad (4.6)$$

Figure 4.8 displays the curve along with the simulation values.

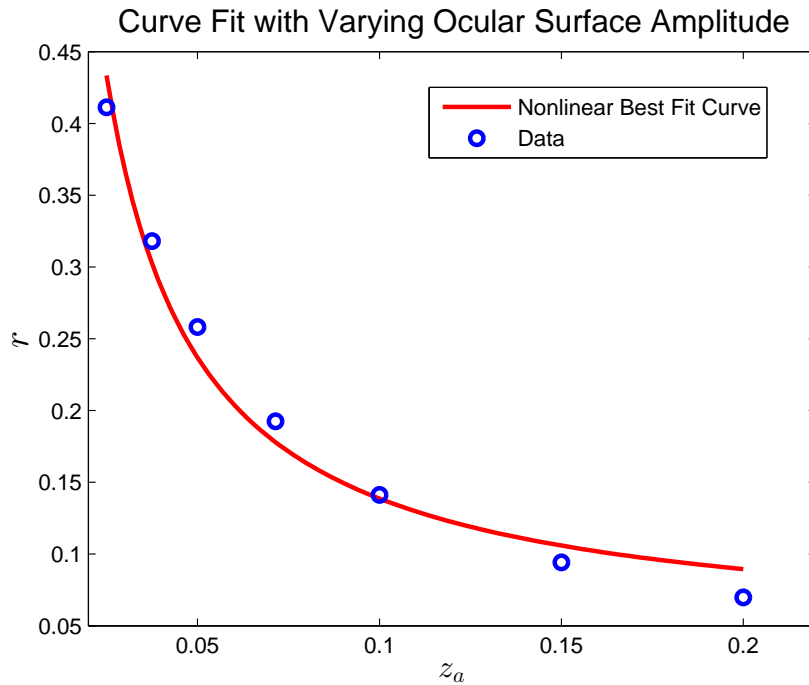


Figure 4.8: Nonlinear curve fit of the ratio values plotted as the red line, with the ratio values plotted as blue circles.

We observed the same behavior in figure 4.8 as in the $k = 10$ case, where that the relative roughness r decreases as we increase the ocular surface amplitude, with the

highest value of r occurring when $z_a = 0.025$. We again explore whether the largest r and largest h_{amp} correspond to the same value of z_a . The results for h_{amp} with varying z_a are displayed in figure 4.9.

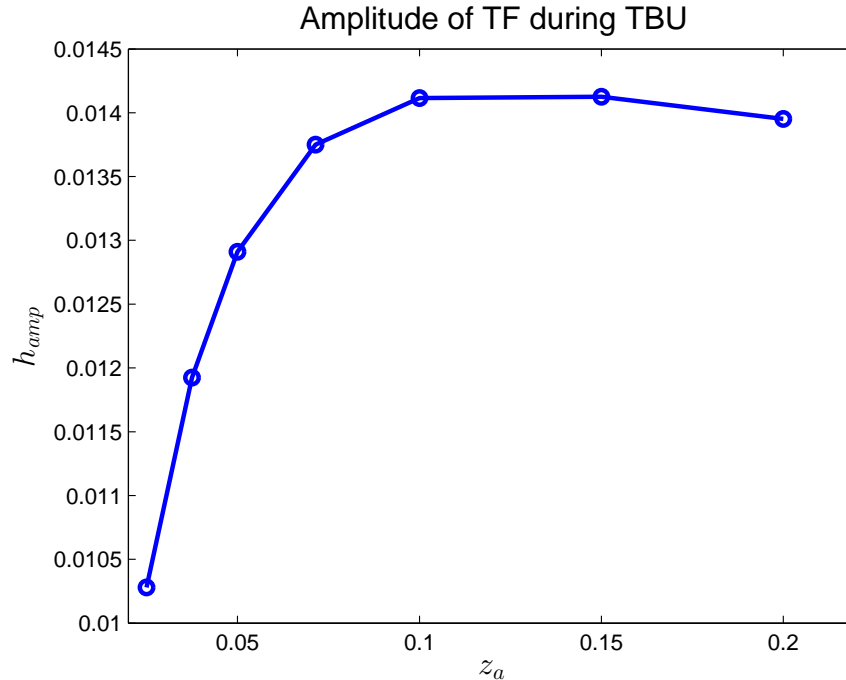


Figure 4.9: Amplitude of the tear film versus the amplitude of the corneal surface when $k = 5$. We obtain the largest amplitude for the ocular surface amplitude $z_a = 0.15$.

Corneal Surface with both Long and Short Waves

In the previous sections, we considered separately cases of longer or shorter waves due to cell division and epithelial erosion. Such biological processes may occur continually and simultaneously [33]. Thus we introduce long and short waves together in order to more realistically mimic the features of the corneal surface. We use the following equation for the ocular surface:

$$z_c(x) = \frac{z_a}{2} [2 + \sin(2\pi k_1 x) + \sin(2\pi k_2 x)]. \quad (4.7)$$

Here $k_1 = 5$ and $k_2 = 20$ represent the long and short waves, respectively. We compute a numerical solution to the model, with the corneal surface given by (4.7). Figure 4.10 displays the final four time steps of the numerical simulation as the tear film nears TBU.

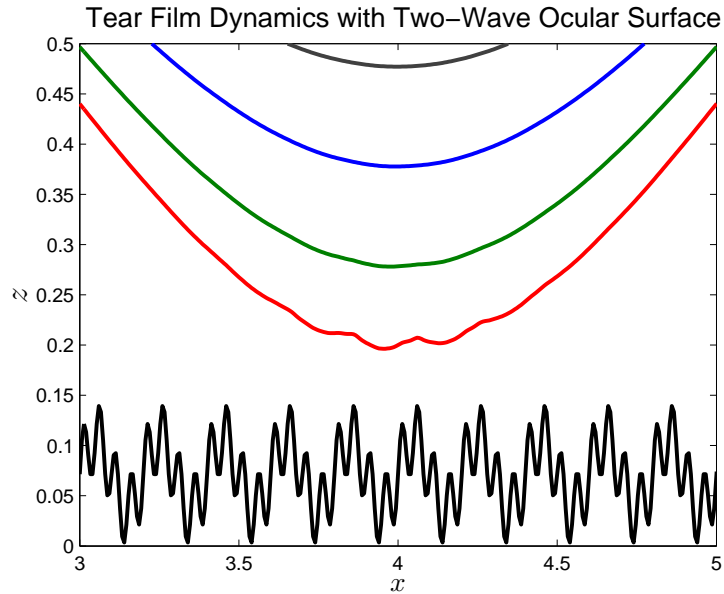


Figure 4.10: Final four time steps (from $t = 0.6$, increasing by 0.1 until final time of $t = 0.8791$) of the tear film in a localized region where TBU occurs, with decreasing thickness throughout time. The tear film ripples in the final time step at TBU, with the wavelength appearing to echo the longer waves ($k_1 = 5$) but not the shorter waves ($k_2 = 20$).

We now solve the PDE for three cases: the two-wave corneal surface, the corneal surface with long wave wavenumber $k = 5$, and the corneal surface with short wave wavenumber $k = 20$. Additionally, we vary the amplitude ranging from $z_a = .05$ to $z_a = .2$. Figure 4.10 suggests that the corneal surface acts as a low pass filter, with the waves in the tear film echoing only the long corneal surface waves but not the short waves. We quantify this effect by calculating representative amplitudes and

wavelengths of the tear film at TBU. The calculated amplitude indicates depth of the tear film ripples, while the calculated wavelength determines whether the long or short waves are reflected in the tear film. We compute the ratio of the tear film amplitude to the corneal surface amplitude, and obtain the results displayed in table 4.1.

z_a	$k = 5$	$k = 20$	two-wave
0.05	0.2582	0.0188	0.1588
0.0714	0.1925	0.0127	0.1033
0.1	0.1411	0.0085	0.0722
0.2	0.0698	0.0034	0.0311

Table 4.1: Ratio of tear film amplitude to corneal surface amplitude ($r = h_{amp}/z_a$) for various ocular surface functions. The amplitude of the tear film corresponding to the two wave corneal surface is larger than the $k = 20$ amplitude and smaller than the $k = 5$ amplitude. This further suggests that the inclusion of shorter waves has a flattening effect.

We also compute an approximate wavenumber of the tear film at TBU to compare it to the wavenumber of the ocular surface. We use the same procedure as previously outlined to find the absolute minimum of the free surface $h + z_c$ and adjacent local maxima. We then find the x coordinates of the maxima, compute their difference d , and take the wavenumber to be $1/d$. Table 4.2 contains wavenumbers of the tear film for varying ocular surface wavenumber and amplitude.

z_a	$k = 5$	$k = 20$	two-wave
.05	4.5455	18.7500	4.0541
.0714	4.5455	18.7500	4.8387
.1	4.5455	18.7500	4.8387
.2	4.5455	18.7500	4.8387

Table 4.2: Wavenumber for various ocular surface functions. We note that these values are approximate due to the numerical discretization process and the fact that the tear film surface is not truly periodic. We observe a longer wave for the two-wave case, close to $k = 5$, and we do not see the $k = 20$ wave.

The wavenumber of the tear film at TBU is found to be almost identical to the wavenumber of the longer wave ($k = 5$). Therefore, the tear film acts as a low pass filter, with its ripples showing the longer waves of the corneal surface and filtering out the shorter waves.

4.2 Effect of Wetting Forces

The fluid pressure is governed largely by the curvature of the fluid surface, given by the $(h + z_c)_{xx}$ term, before the film reaches TBU. This curvature-driven pressure causes the film to decay smoothly with no artifact of the corneal surface. However, as the film gets close to TBU, for example less than 100 nm in some cases, there is a repulsion between the fluid-air interface and the corneal substrate [34, 35]. We describe this repulsion with wetting forces, as experimental studies have shown that the tear film typically wets the corneal surface [36, 37], or in some cases is partially wetting [37]. We account for the wetting forces by including a conjoining pressure function $\Pi(h)$, dependent on the thickness of the film. We first consider a standard form used for van der Waals' forces; then, we consider two modifications that have been proposed

for non-flat substrates [35, 38] such as for our case.

The default wetting forces we consider are the van der Waals' wetting forces, given by (2.48). These forces describe wetting of a thin film of uniform thickness. Nondimensionalizing (2.48), we obtain

$$\Pi(h) = Ah^{-3}, \quad (4.8)$$

where

$$A = \frac{A^*}{6\pi\mu v_0 L^2}. \quad (4.9)$$

Here A^* is the Hamaker constant, with value $A^* = 6\pi \times 3.5 \times 10^{-19} \text{m}^3 \text{Pa}$ [27]. Typical values of A^* range from 10^{-20} to $10^{-19} \text{m}^3 \text{Pa}$ [34].

In the numerical simulations of this section, we use a stopping criterion of $\min_x h(x, t) = 10^{-2}$. We lower the stopping criterion to better observe the effects of wetting forces, which become a dominant force in the pressure function closer to TBU.

Trivial Case: Absence of Wetting Forces

In the case where we do not include a disjoining pressure term, we witness no roughness in the tear film at any point of the simulation, including at TBU. Figure 4.11 shows the dynamics of the thin film without a disjoining pressure. We note that the results of this model are commensurate with previous work on flow over topography, such as [1] and [22], in which fluid flow is driven by external forces such as gravity or blinking and thus yields an artifact of the substrate topography.

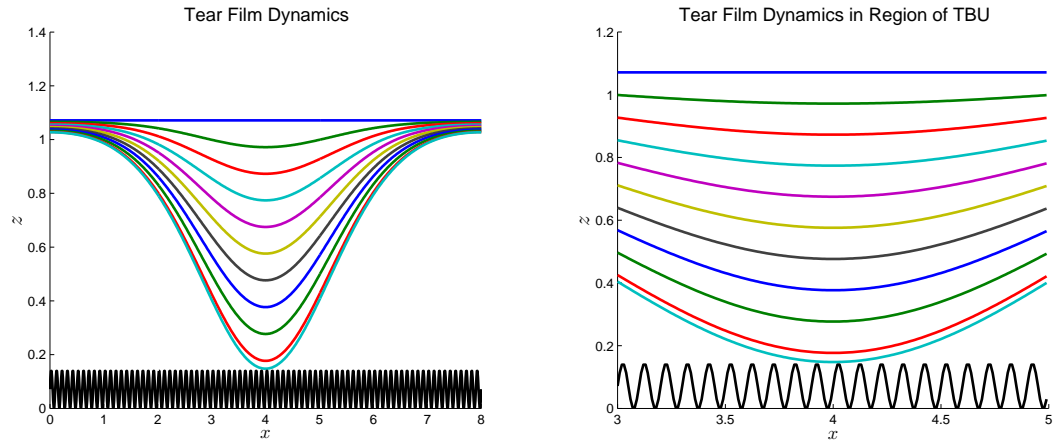


Figure 4.11: Left plot: time series plot of film thickness with absence of wetting forces. Top blue curve is $t = 0$; bottom teal curve is $t = .9291$. The tear film thins until the solver stops it at $h_{min} = 10^{-2}$. In this case, there are no visible ripples in the tear film. Right plot: the same model simulation, zoomed into the localized region at which TBU occurs.

Van der Waals' Forces

We run the model with the default van der Waals' forces given by (4.8). Figure 4.12 displays the progression of the tear film thickness, using an events function to stop the solver at dimensionless thickness of 0.01 (dimensional $0.035\mu\text{m}$).

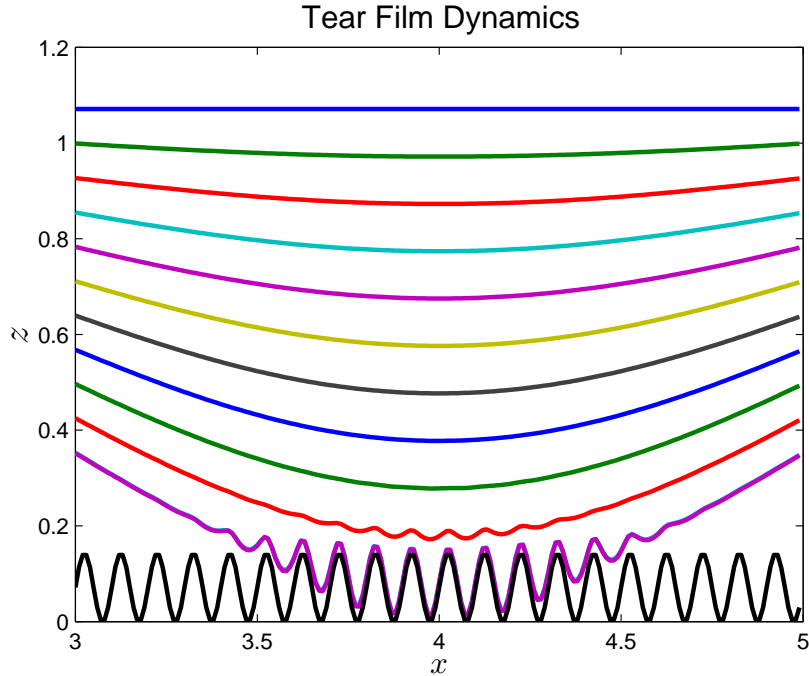


Figure 4.12: Time series plot of film thickness with van der Waals' wetting forces. Top blue curve is $t = 0$; time increases by 0.1 until the bottom purple curve at $t = 1.0015$. The tear film thins until the solver stops it at thickness $h = 10^{-2}$. The wetting forces cause the tear film to spread across the corneal surface at TBU, echoing the shape of the surface.

The roughness of the tear film changed as we varied the wavenumber in the previous section, in the case where the stopping criterion was set $\min_x h(x, t) = 1/14$. We explore the effect of varying wavenumber in figure 4.13 when the stopping criterion is reduced to $\min_x h(x, t) = 10^{-2}$.

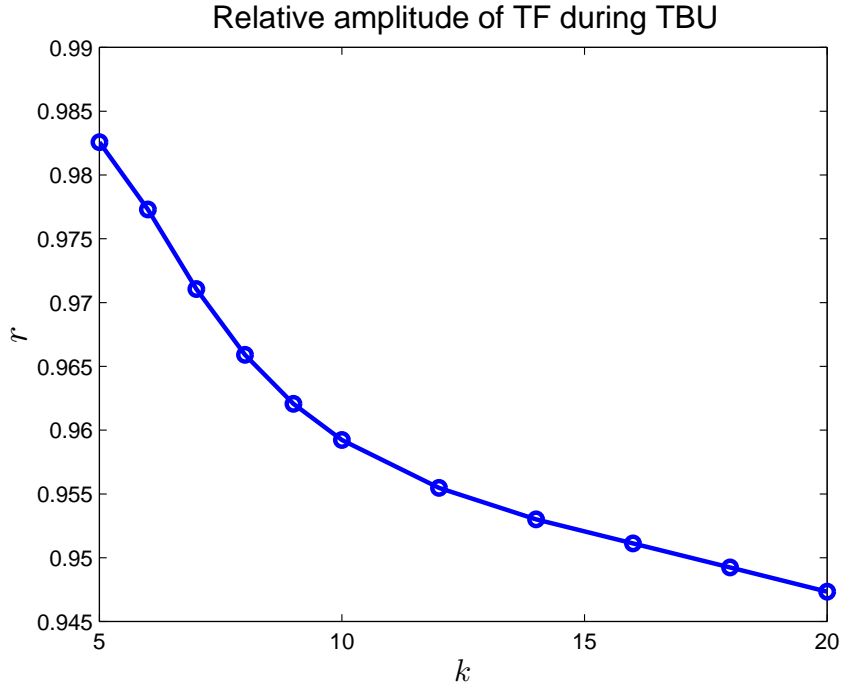


Figure 4.13: Ratio of the tear film amplitude to the corneal surface amplitude as a function of wavenumber when TBU is defined as $\min_x h(x, t) = 10^{-2}$.

Despite variations in the relative amplitude, we note that all plotted values are in the range of $[0.945, 0.985]$ indicating that the tear film wets the corneal surface, closely following its shape at TBU. The results we obtain vary by ± 0.05 based on the chosen grid spacing, due to numerical error in calculation of local maxima. The number of gridpoints represented in figure 4.13 is $N = 10x_L k$.

Disjoining Pressure for Nonuniform Thin Films

Although van der Waals' wetting forces are commonly used in thin film modeling, they are derived for films with two parallel interfaces [39]. We now attempt to use two different disjoining pressure functions that incorporate effects of non-flat surfaces [35, 38]. Given that the model tear film at TBU has a thinner region in the center and thicker regions on the ends, we explore the effect of wetting forces for films of

nonuniform thickness. One such disjoining pressure function for films of nonuniform thickness is derived by Dai, Leal, and Redondo [35]. Dimensionally, it is given by

$$\Pi'(h') = \frac{A^*}{24\pi} h'^{-3} \left[4 - 3 \left(\frac{\partial h'}{\partial x'} \right)^2 + 3h' \frac{\partial^2 h'}{\partial x'^2} \right]. \quad (4.10)$$

We now nondimensionalize (4.10) according to the dimensionless variables established in chapter 2:

$$\frac{v_0\mu}{\varepsilon^2 d} \Pi(h) = \frac{A^*}{24\pi d^3} h^{-3} \left[4 - 3\varepsilon^2 \left(\frac{\partial h}{\partial x} \right)^2 + 3h\varepsilon^2 \frac{\partial^2 h}{\partial x^2} \right] \quad (4.11)$$

Multiplying both sides by $\frac{\varepsilon^2 d}{v_0\mu}$, we have that

$$\Pi(h) = Ah^{-3} \left[1 - \frac{3}{4}\varepsilon^2 \left(\frac{\partial h}{\partial x} \right)^2 + \frac{3}{4}h\varepsilon^2 \frac{\partial^2 h}{\partial x^2} \right]. \quad (4.12)$$

If we drop terms of order ε^2 or greater, we are left with the same disjoining pressure function as that of the van der Waals' forces in (4.8). However, we include the terms involving ε : due to the effect of the pressure function at very small h values, other small terms may come into play.

Upon initial inspection, with the stopping criterion of 10^{-2} , the model with (4.12) seems to behave the same as the model with equation (4.8). We therefore allow the solver to run longer, to check whether there are any qualitative changes at even smaller thicknesses. We reduce the stopping criterion further to $\min_x h(x, t) = 10^{-4}$. In figure 4.14, we display the numerical solutions using (4.12).

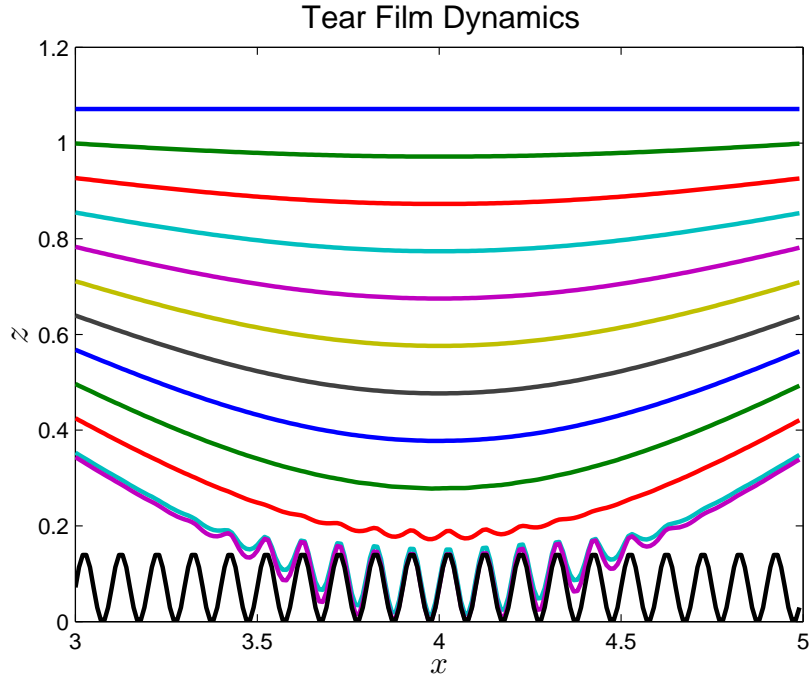


Figure 4.14: Time series plot of film thickness with wetting forces governed by (4.12). Starting with time $t = 0$, we increase by 0.1 until the final time of $t = 1.0134$. We obtain the same behavior with (4.12) as with (4.8).

The results of figure 4.14 do not differ qualitatively from the results with the van der Waals' disjoining pressure equation (4.8). Additionally, each model reaches TBU at the same time, in dimensionless terms, of $t = 1.0134$. To quantify the numerical difference near TBU, we compute the ℓ^2 norm and ℓ^∞ norm of the difference between the values of h in each model at both the penultimate and ultimate time step. See table 4.3 for the values.

Disjoining Pressure with No Movement of Contact Line

An additional physical property to explore with the disjoining pressure is contact line, which is the line where the aqueous layer, outside air, and ocular surface meet. Studies have found a contact angle ranging from 0° (perfectly wetting) to 16° (partial

t	ℓ^2	ℓ^∞
1	1.5×10^{-5}	3.3×10^{-6}
1.0134	1.5×10^{-5}	3.1×10^{-6}

Table 4.3: Comparison of van der Waals' disjoining pressure, and Dai et al.'s disjoining pressure for films of nonuniform thickness.

wetting) [37]. Here we make an initial exploration into incorporating partial wetting. For the case of partial wetting, in many instances one wishes to prevent movement of the contact line due to no-slip conditions at the corneal surface. We incorporate into our model the following disjoining pressure function, as given dimensionally by Wu and Wong [38]:

$$\Pi'(h') = Bh'^{-3} \left(\alpha^4 - \frac{\partial h'^4}{\partial x'} + 2h' \frac{\partial h'^2}{\partial x'} \frac{\partial^2 h'}{\partial x'^2} \right). \quad (4.13)$$

We nondimensionalize according to the dimensionless variables given in chapter 2:

$$\frac{v_0\mu}{\varepsilon^2 d} \Pi(h) = Bd^{-3} h^{-3} \left(\alpha^4 - \varepsilon^4 \frac{\partial h}{\partial x} + 2h\varepsilon^4 \frac{\partial h^2}{\partial x} \frac{\partial^2 h}{\partial x^2} \right). \quad (4.14)$$

Multiplying both sides by $\frac{\varepsilon^2 d}{v_0\mu}$, we obtain the following dimensionless equation corresponding to (4.13):

$$\Pi(h) = \frac{B}{L^2 v_0 \mu} h^{-3} \left(\alpha^4 - \varepsilon^4 \frac{\partial h}{\partial x} + 2h\varepsilon^4 \frac{\partial h^2}{\partial x} \frac{\partial^2 h}{\partial x^2} \right). \quad (4.15)$$

We note that for $\alpha = 0^\circ$ which represents the perfectly wetting case, we trivially satisfy the condition of no moving contact line. In this case, the model is virtually absent of a disjoining pressure, with the exception of terms involving ε^4 . This absence of a disjoining pressure is not consistent with the terms required in the model for the perfectly wetting case. Moreover, when attempting to solve the model numerically at $\alpha = 0^\circ$, the solver breaks before reaching a low enough thickness to observe the effects of disjoining pressure. When $\alpha = 16^\circ$ in the partial wetting case, we face a similar issue, in which the solver returns erroneous plots once reaching a TBU-level thickness. Therefore, the effect of (4.15) on our model is inconclusive.

Chapter 5

DISCUSSION AND CONCLUSIONS

We recall experimental images such as figure 1.3 in which we observe areas of rough texture. Our work was motivated by the interpretation of such images, and we put our results in context based on such images. Our results support the interpretation of rough regions as TBU, given that the model tear film develops ripples at but not before TBU. These ripples vary in amplitude and wavenumber based on the features of the ocular surface and glycocalyx. In the case of a healthy glycocalyx, i.e. when the stopping criterion is set to $0.25\mu\text{m}$, the tear film roughness varies from about 1% to 20% of the amplitude of the corneal surface, with higher amplitude for lower wavenumber ocular surface. At 20% the amplitude of the corneal surface, the tear film amplitude is $0.05\mu\text{m}$, compared to the average epithelial cell height of $0.25\mu\text{m}$ and average epithelial cell width of $35\mu\text{m}$. When the tear film thins below the glycocalyx to $0.035\mu\text{m}$, the tear film hugs the corneal surface, echoing its amplitude and wavenumber. We also find that in a corneal surface with long and short waves, the tear film ripples echo the wavelength of the long waves, with an amplitude between the long and short wave cases. This suggests that the tear film acts as a low pass filter, only reflecting the shape of the long waves.

Our results differ qualitatively from previous results involving a rough ocular surface, such as those of Braun et al. [1]. They modeled tear film dynamics during a blink with a rough ocular surface, in which case the dynamics were flow-driven by the moving eyelid boundary. Due to the lateral fluid flow in their model, the shape of the rough ocular surface was evident even at healthy film thickness. However, we model dynamics during interblink, when the eyelid does not move and flow is not driven by a

blink. The curvature of the free surface, which is initialized to be smooth, dominates the pressure gradient for higher h , or thicker aqueous layer. Only at smaller h , as we reach TBU, do wetting forces appear strong enough to form ripples in the tear film.

The inclusion of wetting forces at lower aqueous layer thickness was crucial in the formation of tear film ripples at TBU. With van der Waals' wetting forces, we achieved the same behavior as with the wetting forces for films of nonuniform thickness found in [35]. Because of the aspect ratio of our problem, the additional terms involving the tear film curvature did not come into play in our model. When attempting to account for no movement of contact line with a conjoining pressure equation from [38], the solver broke before reaching TBU-level thicknesses. This equation also was greatly simplified because of the small height to length ratio in our model, which likely affected the results.

One of the many challenges of our model is the shortage of information about the corneal surface. While we model tear film roughness based on corneal surface properties, current imaging techniques do not provide simultaneous data on tear film thickness and corneal surface features. We therefore combined data such as average epithelial cell height and width, along with an experimentally-derived standard deviation of $0.129\mu\text{m}$ for corneal surface roughness [7], to establish an appropriate range of parameter values in our simulations. If we center the amplitude around the average epithelial cell height of $0.25\mu\text{m}$, then using the standard deviation from [7], we have that 95% of corneal surface amplitudes will be in the range from $0\mu\text{m}$ (flat) to $0.508\mu\text{m}$. Our chosen amplitude values vary from a flat corneal surface to $0.7\mu\text{m}$, therefore closely replicating the variance found by [7]. We similarly vary wavenumber centered around the average epithelial cell width, although we do not have data on the standard deviation of width.

There are several future directions we can take to improve our model. We

can incorporate properties of experimental imaging into our model, in order to form a more direct comparison between simulation and experiment. Current models such as [40] introduce fluorescein concentration as a variable; we can add fluorescein to our model although we do not expect to observe tear film rippling experimentally using fluorescein imaging. It would be more appropriate, albeit more challenging, to incorporate interferometry into our model. Other improvements could be to include more physical properties of the system, such as osmosis at the corneal surface boundary, and measuring osmolarity of the aqueous layer. Both osmosis and osmolarity drive fluid flow and thus may change the tear film dynamics. We can also incorporate the features of the glycocalyx into our model. The glycocalyx protrudes from the ocular surface into the aqueous layer; including it in the model will likely influence dynamics at TBU that are relevant to surface topography. Lastly, we can extend our one-dimensional model to a model with a two-dimensional ocular surface and two-dimensional tear film.

BIBLIOGRAPHY

- [1] R. J. Braun, P. E. King-Smith, C. G. Begley, L. Li, and N. R. Gewecke. Dynamics and function of the tear film in relation to the blink cycle. *Prog. Retin. Eye Res.*, 45:132–164, 2015.
- [2] P. E. King-Smith, J. J. Nichols, K. K. Nichols, B. A. Fink, and R. J. Braun. Contributions of evaporation and other mechanisms to tear film thinning and breakup. *Optom. Vis. Sci.*, 85:623–630, 2008.
- [3] S. Mishima and D. M. Maurice. The oily layer of the tear film and evaporation from the corneal surface. *Exp. Eye Res.*, 1:39–45, 1961.
- [4] I. K. Gipson. Distribution of mucins at the ocular surface. *Exp. Eye Res.*, 78:379–388, 2004.
- [5] M. Hogan, J. Alvarado, and J. Weddell. *Histology of the Human Eye: An Atlas and Textbook*. W. B. Saunders Company, Philadelphia, 1971.
- [6] A. C. Romano, E. M. Espana, S. H. Yoo, M. T. Budak, J. M. Wolosin, and S. C. G. Tseng. Different cell sizes in human limbal and central corneal basal epithelia measured by confocal microscopy and flow cytometry. *Investigative ophthalmology & visual science*, 44(12):5125–5129, 2003.
- [7] P. E. King-Smith, S. H. Kimball, and J. J. Nichols. Tear film interferometry and corneal surface roughness. *Invest. Ophthalmol. Vis. Sci.*, 55(4):2614, 2014.
- [8] *Dry Eye Syndrome – Carlin Vision*. [Online]. Available from <https://www.carlinvision.com/our-services/eye-care/dry-eyes/>. [Accessed March 15, 2016].
- [9] S. Mishima. Some physiological aspects of the precorneal tear film. *Archives of ophthalmology*, 73(2):233–241, 1965.
- [10] P. E. King-Smith, B. A. Fink, N. Fogt, K. K. Nichols, R. M. Hill, and G. S. Wilson. The thickness of the human precorneal tear film: Evidence from reflection spectra. *Invest. Ophthalmol. Vis. Sci.*, 41:3348–3359, 2000.
- [11] A. Sharma and E. Ruckenstein. The role of lipid abnormalities, aqueous and mucus deficiencies in the tear film breakup, and implications for tear substitutes and contact lens tolerance. *J. Coll. Interface Sci.*, 111:456–479, 1986.

- [12] Anonymous. Report of the International Dry Eye WorkShop (DEWS). *Ocul. Surf.*, 5:65–204, 2007.
- [13] S. P. Lin and H. Brenner. Marangoni convection in a tear film. *Journal of Colloid and Interface Science*, 85(1):59–65, 1982.
- [14] R. J. Braun and A. D. Fitt. Modeling the drainage of the precorneal tear film after a blink. *Math. Med. Biol.*, 20:1–28, 2003.
- [15] S. H. Kimball, P. E. King-Smith, and J. J. Nichols. Evidence for the major contribution of evaporation to tear film thinning between blinks. *Invest. Ophthalmol. Vis. Sci.*, 51:6294–6297, 2010.
- [16] P. E. King-Smith, J. J. Nichols, R. J. Braun, and K. K. Nichols. High resolution microscopy of the lipid layer of the tear film. *The ocular surface*, 9(4):197–211, 2011.
- [17] C.-C. Peng, C. Cerretani, R. J. Braun, and C. J. Radke. Evaporation-driven instability of the precorneal tear film. *Adv. Coll. Interface Sci.*, 206:250–264, 2014.
- [18] R. J. Braun. Dynamics of the tear film. *Annu. Rev. Fluid Mech.*, 44:267–297, 2012.
- [19] R. V. Craster and O. K. Matar. Dynamics and stability of thin liquid films. *Rev. Mod. Phys.*, 81:1131–1198, 2009.
- [20] S. Kalliadasis, C. Bielarz, and G. M. Homsy. Steady free-surface thin film flows over topography. *Physics of Fluids (1994-present)*, 12(8):1889–1898, 2000.
- [21] S. Kalliadasis and G. M. Homsy. Stability of free-surface thin-film flows over topography. *Journal of Fluid Mechanics*, 448:387–410, 2001.
- [22] A. Wierschem, M. Scholle, and N. Aksel. Comparison of different theoretical approaches to experiments on film flow down an inclined wavy channel. *Experiments in fluids*, 33(3):429–442, 2002.
- [23] B. Nagyová and J. M. Tiffany. Components of tears responsible for surface tension. *Curr. Eye Res.*, 19:4–11, 1999.
- [24] J. M. Tiffany. The viscosity of human tears. *Int. Ophthalmol.*, 15:371–376, 1991.
- [25] J. J. Nichols, G. L. Mitchell, and P. E. King-Smith. Thinning rate of the precorneal and prelens tear films. *Invest. Ophthalmol. Visual Sci.*, 46:2353–2361, 2005.
- [26] D. J. Acheson. *Elementary fluid dynamics*. Oxford University Press, 1990.

- [27] K. N. Winter, D. M. Anderson, and R. J. Braun. A model for wetting and evaporation of a post-blink precorneal tear film. *Math. Med. Biol.*, 27:211–225, 2010.
- [28] A. Oron, S. H. Davis, and S. G. Bankoff. Long-scale evolution of thin liquid films. *Reviews of modern physics*, 69(3):931, 1997.
- [29] MATLAB Release 2014a, The MathWorks, Inc., Natick, Massachusetts, United States.
- [30] L. N. Trefethen. *Spectral Methods in MATLAB*. SIAM, Philadelphia, 2000.
- [31] U. M. Ascher and L. R. Petzold. *Computer methods for ordinary differential equations and differential-algebraic equations*, volume 61. Siam, 1998.
- [32] B. Govindarajan and I. K. Gipson. Membrane-tethered mucins have multiple functions on the ocular surface. *Exp. Eye Res.*, 90:655–693, 2010.
- [33] A. J. Bron, P. Argüeso, M. Irkeç, and F. V. Bright. Clinical staining of the ocular surface: Mechanisms and interpretations. *Prog. Ret. Eye Res.*, 78:36–61, 2015.
- [34] L. G. Leal. *Advanced transport phenomena: fluid mechanics and convective transport processes*. Cambridge University Press, 2007.
- [35] B. Dai, L. G. Leal, and A. Redondo. Disjoining pressure for nonuniform thin films. *Physical Review E*, 78(6):061602, 2008.
- [36] J. M. Tiffany. Measurement of wettability of the corneal epithelium I. particle attachment method. *Acta Ophthalmol.*, 68:175–181, 1990.
- [37] J. M. Tiffany. Measurement of wettability of the corneal epithelium II. contact angle method. *Acta Ophthalmol.*, 68:182–187, 1990.
- [38] Q. Wu and H. Wong. A slope-dependent disjoining pressure for non-zero contact angles. *Journal of Fluid Mechanics*, 506:157–185, 2004.
- [39] J. N. Israelachvili. *Intermolecular and surface forces: revised third edition*. Academic press, 2011.
- [40] R. J. Braun, T. A. Driscoll, C. G. Begley, P. E. King-Smith, and J. I Siddique. On tear film breakup (tbu): Dynamics and imaging. *Math. Med. Biol.*, Under revision:1–40, 2016.

Appendix A
PERMISSION LETTERS

A.1 Permission from Wolters Kluwer Health

This Agreement between Amy Janett ("You") and Wolters Kluwer Health, Inc. ("Wolters Kluwer Health, Inc.") consists of your license details and the terms and conditions provided by Wolters Kluwer Health, Inc. and Copyright Clearance Center.

License Number 3897710795992

License date Jun 28, 2016

Licensed Content Publisher Wolters Kluwer Health, Inc.

Licensed Content Publication Optometry and Vision Science

Licensed Content Title Contributions of Evaporation and Other Mechanisms to Tear Film Thinning and Break-Up

Licensed Content Author P King-Smith, Jason Nichols, Kelly Nichols, et al

Licensed Content Date Jan 1, 2008

Licensed Content Volume Number 85

Licensed Content Issue Number 8

Type of Use Dissertation/Thesis

Requestor type Individual

Portion Figures/table/illustration

Number of figures/tables/illustrations 1

Figures/tables/illustrations used 3A

Author of this Wolters Kluwer article No

Title of your thesis / dissertation Tear Film Dynamics in Breakup with a Rough Ocular Surface

Expected completion date Jul 2016

Estimated size(pages) 65

Requestor Location Amy Janett

15 Orchard Rd

NEWARK, DE 19716

United States

Terms and Conditions

Wolters Kluwer Terms and Conditions

Transfer of License: Wolters Kluwer hereby grants you a non-exclusive license to reproduce this material for this purpose, and for no other use, subject to the conditions herein.

Credit Line: will be prominently placed and include: For books the author(s), title of book, editor, copyright holder, year of publication; For journals the author(s), title of article, title of journal, volume number, issue number and inclusive pages. Warranties: The requestor warrants that the material shall not be used in any manner which may be considered derogatory to the title, content, or authors of the material, or to Wolters Kluwer.

Indemnity: You hereby indemnify and hold harmless Wolters Kluwer and their respective officers, directors, employees and agents, from and against any and all claims, costs, proceeding or demands arising out of your unauthorized use of the Licensed Material.

Geographical Scope: Permission granted is non-exclusive, and is valid throughout the world in the English language and the languages specified in your original request. Wolters Kluwer cannot supply the requestor with the original artwork, electronic files or a "clean copy."

Permission is valid if the borrowed material is original to a Wolters Kluwer imprint (Lippincott-Raven Publishers, Williams & Wilkins, Lea & Febiger, Harwal, Rapid

Science, Little Brown & Company, Harper & Row Medical, American Journal of Nursing Co, and Urban & Schwarzenberg - English Language, Raven Press, Paul Hoeber, Springhouse, Ovid).

Termination of contract: If you opt not to use the material requested above please notify RightsLink or Wolters Kluwer within 90 days of the original invoice date.

This permission does not apply to images that are credited to publications other than Wolters Kluwer books/journals or its Societies. For images credited to non-Wolters Kluwer books or journals, you will need to obtain permission from the source referenced in the figure or table legend or credit line before making any use of the image(s) or table(s). Modifications: With the exception of text size or color, no Wolters Kluwer material is permitted to be modified or adapted without publisher approval.

Third party material: Adaptations are protected by copyright, so if you would like to reuse material that we have adapted from another source, you will need not only our permission, but the permission of the rights holder of the original material. Similarly, if you want to reuse an adaptation of original LWW content that appears in another publishers work, you will need our permission and that of the next publisher. The adaptation should be credited as follows: Adapted with permission from Wolters Kluwer: Book author, title, year of publication or Journal name, article author, title, reference citation, year of publication. Modifications are permitted on an occasional basis only and permission must be sought by Wolters Kluwer.

Duration of the license: Permission is granted for a one-time use only within 12 months from the date of this invoice. Rights herein do not apply to future reproductions, editors, revisions, or other derivative works. Once the 12 - month term has expired, permission to renew must be submitted in writing.

For content reused in another journal or book, in print or electronic format, the license is one-time use and lasts for the 1st edition of a book or for the life of the edition in case of journals.

If your Permission Request is for use on a website (which is not a journal or a book), internet, intranet, or any publicly accessible site, you agree to remove the material

from such site after 12 months or else renew your permission request.

Contingent on payment: While you may exercise the rights licensed immediately upon issuance of the license at the end of the licensing process for the transaction, provided that you have disclosed complete and accurate details of your proposed use, no license is finally effective unless and until full payment is received from you (either by publisher or by CCC) as provided in CCC's Billing and Payment terms and conditions. If full payment is not received on a timely basis, then any license preliminarily granted shall be deemed automatically revoked and shall be void as if never granted. Further, in the event that you breach any of these terms and conditions or any of CCC's Billing and Payment terms and conditions, the license is automatically revoked and shall be void as if never granted. Use of materials as described in a revoked license, as well as any use of the materials beyond the scope of an unrevoked license, may constitute copyright infringement and publisher reserves the right to take any and all action to protect its copyright in the materials. **Waived permission fee:** If the permission fee for the requested use of our material has been waived in this instance, please be advised that your future requests for Wolters Kluwer materials may incur a fee.

Service Description for Content Services: Subject to these terms of use, any terms set forth on the particular order, and payment of the applicable fee, you may make the following uses of the ordered materials:

Content Rental: You may access and view a single electronic copy of the materials ordered for the time period designated at the time the order is placed. Access to the materials will be provided through a dedicated content viewer or other portal, and access will be discontinued upon expiration of the designated time period. An order for Content Rental does not include any rights to print, download, save, create additional copies, to distribute or to reuse in any way the full text or parts of the materials.

Content Purchase: You may access and download a single electronic copy of the materials ordered. Copies will be provided by email or by such other means as publisher may make available from time to time. An order for Content Purchase does not include any rights to create additional copies or to distribute copies of the materials.

A.2 Permission from Elsevier

This Agreement between Amy Janett ("You") and Elsevier ("Elsevier") consists of your license details and the terms and conditions provided by Elsevier and Copyright Clearance Center.

License Number 3897711101403

License date Jun 28, 2016

Licensed Content Publisher Elsevier

Licensed Content Publication Progress in Retinal and Eye Research

Licensed Content Title Dynamics and function of the tear film in relation to the blink cycle

Licensed Content Author R.J. Braun,P.E. King-Smith,C.G. Begley,Longfei Li,N.R. Gewecke

Licensed Content Date March 2015

Licensed Content Volume Number 45

Licensed Content Issue Number n/a

Licensed Content Pages 33

Start Page 132

End Page 164

Type of Use reuse in a thesis/dissertation

Intended publisher of new work other

Portion figures/tables/illustrations

Number of figures/tables/illustrations 2

Format both print and electronic

Are you the author of this Elsevier article? No

Will you be translating? No

Order reference number Original figure numbers figures 1, 26

Title of your thesis/dissertation Tear Film Dynamics in Breakup with a Rough Ocular Surface

Expected completion date Jul 2016

Estimated size (number of pages) 65

Requestor Location Amy Janett

15 Orchard Rd

NEWARK, DE 19716

United States

Terms and Conditions

INTRODUCTION

1. The publisher for this copyrighted material is Elsevier. By clicking "accept" in connection with completing this licensing transaction, you agree that the following terms and conditions apply to this transaction (along with the Billing and Payment terms and conditions established by Copyright Clearance Center, Inc. ("CCC"), at the time that you opened your Rightslink account and that are available at any time at <http://myaccount.copyright.com>).

GENERAL TERMS

2. Elsevier hereby grants you permission to reproduce the aforementioned material subject to the terms and conditions indicated.

3. Acknowledgement: If any part of the material to be used (for example, figures) has appeared in our publication with credit or acknowledgement to another source, permission must also be sought from that source. If such permission is not obtained then that material may not be included in your publication/copies. Suitable acknowledgement to the source must be made, either as a footnote or in a reference list at the end of your publication, as follows:

"Reprinted from Publication title, Vol /edition number, Author(s), Title of article / title of chapter, Pages No., Copyright (Year), with permission from Elsevier [OR APPLICABLE SOCIETY COPYRIGHT OWNER]." Also Lancet special credit - "Reprinted from The Lancet, Vol. number, Author(s), Title of article, Pages No., Copyright (Year), with permission from Elsevier."

4. Reproduction of this material is confined to the purpose and/or media for which

permission is hereby given.

5. Altering/Modifying Material: Not Permitted. However figures and illustrations may be altered/adapted minimally to serve your work. Any other abbreviations, additions, deletions and/or any other alterations shall be made only with prior written authorization of Elsevier Ltd. (Please contact Elsevier at permissions@elsevier.com)

6. If the permission fee for the requested use of our material is waived in this instance, please be advised that your future requests for Elsevier materials may attract a fee.

7. Reservation of Rights: Publisher reserves all rights not specifically granted in the combination of (i) the license details provided by you and accepted in the course of this licensing transaction, (ii) these terms and conditions and (iii) CCC's Billing and Payment terms and conditions.

8. License Contingent Upon Payment: While you may exercise the rights licensed immediately upon issuance of the license at the end of the licensing process for the transaction, provided that you have disclosed complete and accurate details of your proposed use, no license is finally effective unless and until full payment is received from you (either by publisher or by CCC) as provided in CCC's Billing and Payment terms and conditions. If full payment is not received on a timely basis, then any license preliminarily granted shall be deemed automatically revoked and shall be void as if never granted. Further, in the event that you breach any of these terms and conditions or any of CCC's Billing and Payment terms and conditions, the license is automatically revoked and shall be void as if never granted. Use of materials as described in a revoked license, as well as any use of the materials beyond the scope of an unrevoked license, may constitute copyright infringement and publisher reserves the right to take any and all action to protect its copyright in the materials.

9. Warranties: Publisher makes no representations or warranties with respect to the licensed material.

10. Indemnity: You hereby indemnify and agree to hold harmless publisher and CCC, and their respective officers, directors, employees and agents, from and against any and all claims arising out of your use of the licensed material other than as specifically

authorized pursuant to this license.

11. No Transfer of License: This license is personal to you and may not be sublicensed, assigned, or transferred by you to any other person without publisher's written permission.

12. No Amendment Except in Writing: This license may not be amended except in a writing signed by both parties (or, in the case of publisher, by CCC on publisher's behalf).

13. Objection to Contrary Terms: Publisher hereby objects to any terms contained in any purchase order, acknowledgment, check endorsement or other writing prepared by you, which terms are inconsistent with these terms and conditions or CCC's Billing and Payment terms and conditions. These terms and conditions, together with CCC's Billing and Payment terms and conditions (which are incorporated herein), comprise the entire agreement between you and publisher (and CCC) concerning this licensing transaction. In the event of any conflict between your obligations established by these terms and conditions and those established by CCC's Billing and Payment terms and conditions, these terms and conditions shall control.

14. Revocation: Elsevier or Copyright Clearance Center may deny the permissions described in this License at their sole discretion, for any reason or no reason, with a full refund payable to you. Notice of such denial will be made using the contact information provided by you. Failure to receive such notice will not alter or invalidate the denial. In no event will Elsevier or Copyright Clearance Center be responsible or liable for any costs, expenses or damage incurred by you as a result of a denial of your permission request, other than a refund of the amount(s) paid by you to Elsevier and/or Copyright Clearance Center for denied permissions.